FACULTY OF INFORMATION TECHNOLOGY AND ELECTRICAL ENGINEERING

Arman Mansouri Serenjianeh

SATELLITE IMAGE ANALYSIS FOR ENVIRONMENT STUDIES

Master's Thesis
Degree Programme in Computer Science and Engineering
June 2021

Mansouri Serenjianeh A. (2021) Satellite Image Analysis for Environment Studies. University of Oulu, Degree Programme in Computer Science and Engineering, 63 p.

ABSTRACT

In Finnish gold mining, passive treatment plays a significant role in filtration of mining-influenced water, which has important impacts on aquatic and terrestrial ecosystems such as peatlands. The unstable and unpredictable natural factors and parameters such as temperature, sunlight, and rainfall during gold extraction, have made the analysis of the mine operation impact assessment (MOIA) very challenging, which calls for further research on the issue. This study uses remote sensing data from a reference area to test a new technique for MOIA. The approach makes use of the normalized difference vegetation index (NDVI) of images captured from Landsat satellites, before and during the operation of gold mine from the impacted peatlands and surrounding areas, followed by a correlation analysis and impact assessment. The results demonstrate the feasibility of the apprach to predict the status of peatlands in the vicinity of the mining site. The analysis also showed the influence of the temperature and water treatment operation on the target peatlands, which can pave the way for the development of future MOIA tools for peatland drainage.

Keywords: Mine operation impact assessment (MOIA), water treatment, NDVI, Correlation.

TABLE OF CONTENTS

LIST OF FIGURES AND TABLES

-

FOREWORD

The idea behind this research originally stemmed from my passion for developing the Artificial Intelligence or AI techniques such as machine learning and image processing approaches in other sciences. As the world moves further into the digital age, the manual processing will be replaced with automatically methods based on AI, which are faster and more accurate compare to the human activities. One of the fields that can be more time consuming in manual processing is analyzing remote sensing data, which include a vast amount of content. Hence, creating an automate analyzation would be essential, and gave me this motivation to hire the AI approaches in analyzing remote sensing data.

In actual fact, without a strong support group, there was not this ability for me to achieve my current level of success. Since, first of all, I would like to thank my supervisor, Prof. Mourad Oussalah for his support. A special thanks to Dr. Ali Torabi Haghighi for providing materials and feedback based on his experience and knowledge. I also thank Water, Energy and Environmental Engineering Research Unit (University of Oulu) for providing generous funding. Lastly, I would like to thank my family and my friends for their support and motivation through difficult experiences during the global pandemic.

Oulu, June 7th, 2021

Arman Mansouri Serenjianeh

LIST OF ABBREVIATIONS AND SYMBOLS

CSE	Computer Science and Engineering
NDVI	Normalized Difference Vegetation Index
$NDVI_{el}$	Estimated Normalized Difference Vegetation Index
$NDVI_{il}$	Impacted Normalized Difference Vegetation Index
RC	Relative Change
ED	Euclidean distance
MOIA	mine operation impact assessment
$\mathbf{T}$	Determinant of a Matrix
σ	standard deviation
μ	mean
p_{ij}	pixel
t	time
$\mathbf{r}$	Pearson Coefficient
$\lfloor \rfloor$	integer part
$\sum$	sum
$\%$	reminder

1. INTRODUCTION

The mining tradition in Finland is rooted back in early fifties. The operation of the first iron extraction is dated back to the 1950s in the south of Finland where more than thousand mine operations were used to extract minerals and metal ores for various industries, which contributed to the development of Finnish industry in subsequent years [1][2]. Raw materials are seen essential in the industries of metal, chemical and paper. IN parallel, metals such as gold, chrome, nickel, copper and zinc were extracted from northern, southern and eastern parts of Finland [3]. On the other hand, the Finnish mining industry is cyclical, and it is completely influenced by global price, and other economical factors, although an increasing trend is noticed since last decades [4].Therefore, it is predicted that the number of ore and minerals mining would raise to 70 million tons from 4 million tons in 10 years, and the number of persons, who work in mining industry either directly or indirectly, will increase as well by a large margin [1][5].

While the industry of metal exploration has impact on economy, the surrounding environment is often negatively impacted by the mine [6][3]. Especially, mine sites in Finland are often surrounded by forests and peatlands, and because of cold climate in regions such as Arctic and sub-Arctic, the pollutants persist longer in the soil [7]. Accordingly, the management of environmental matters to prevent harmful impacts of mine operation on environments is essential [3]. One of the environments, which has been analyzed with the impacts of mine operation, is the Lake of Jormasjärvi, which has experienced a substantial shift of its water biological properties since 2010 [8]. This partly motivates our interest in this study to focus water ecosystem in the vicinity of the goldmine.

A large amount of water is required in mining operations for drilling, slurry, chemical handling, washing equipment, among other operations. Such a water is extracted from either lake or river. In addition, part of the water used in this mining operations cannot be recycled and is known as a wastewater [3]. This is also referred as mining-influenced water, mining-affected water or mine water. To describe the process of dewatering or drainage water, the mining-influenced water is going to be used. This output water, which is influenced by mining operation, based on mining methods and metal types could contain harmful substances such as metals (Cr, Cu, Pb, Mo, Ni, Zn, V, U, Fe, Al), metalloids (arsenic, antimony), nutrients (nitrogen compounds) and salts (chlorides, cyanides and etc) [3][9][10].

However, the water usages of mines are not completely separated from fresh water sources, and some parts of it could be recycled and reused. Table 1 shows the proportions of fresh water and recycled water used by some ore mines in Finland.

Table 1. Some metal ore mines' water usage in Finland in 2009 [3]

Name of the mine	Water consumption (cubic meter per year)	Fresh water's source	The methods of recycling	The percentage of recycling step
Kittilä	1,000,000	Seurujoki River	Tailing ponds	65-70%
Kemi[1]	2,546,900	Settling pond	Settling pond	98%
Pyhäsalmi	4,970,000	Pyhäjärvi lake	Thickening process	18%
Talvivaara	1,360,000	Kolmisoppi järvi lake	Gypsum precipitate ponds	10-20%
Vammala	1,200,000	The water which was recirculated	Tailing ponds	100%
Lahnaslampi	800,000	Dewatering from the mine	Dewatering from the mine and Tailing ponds	>90%

For treating water from mine operation two methods, referred to as passive and active are distinguished. The goal in both treatments is discharging acidity and metals from mining-influenced water [11]. Table 2 illustrates some active treatment technologies, which have been used to treat water. Common challenges associated to active water treatment are mainly concerned with water management issues, the process of separating solid from liquid, lack of water stability, conditions of climate and maintenance and administration of operation cost based on day-to-day [12]. On the other hand, passive treatments could be used as alternative methods where low acidity, low rates of float and low acidity loads can be inferred [13].

[3]data belongs 2008

Table 2. Some examples of active treatment of water[14][15][16][17]

Used active methods in water's treatment	Natural or chemical composite for active treatment
Nitrogen discharge	Adding a bacteria named anammox and CO_2
Sulphate discharge	Chemical precipitation: adding barium or calcium salts and Physical
Alkali-activation (or geopolymer)	Aluminosilicate precursors
Wastewater treatment with artificial aeration	—-

In recent years, passive treatments have been popular in water treatment process [18][19], which include a series of intermediate steps [20]. Table 3 shows some examples of passive treatment used in cold climate [21], where wetland is acknowledged as a distinguished treatment

Table 3. Some examples of passive treatment of water[22][23][24]

Name of passive treatment	The operation
Anoxic limestone drains (ALDs)	Burying the limestone's beds to remove acid mine
Wetland	Ameliorating mine drainage
Reactive barrier	Mine water is directed to a ditch, which includes cow manure, leaf, and etc.

The advantage list of wetland treatment includes low energy and low operational cost, which made the process effective for small or remote environment [25]. From the end of 1980s, one of goals in using wetland treatment has been the performance of forest drainage and peat harvesting [21] as well as the the improvement in water quality and nutrient reduction in aquatic systems [26][27][15].

Especially, the peat soil capacity enables us to remove metals and metalloids from water, since peatlands are being used as a buffer and the last process of the mining-influenced water treatment pipeline [28][29][30][31][32]. This removal operation occurs as a result of changes of ion, complexation and chemisorption during the process of surface-absorbate species exchange [33].

Still, the question whether there is a balance between the advantages of using peatlands as a water treatment and the damages induced during the absorption process of water bodies in the peatlands is worth considering. Indeed, peatlands include a

variety of flora and fauna acting as complex ecosystems [34][35][36]. Since flora and fauna can be damaged or destroyed with the properties of mining-influenced water, this, in turn, can impact the peatland natural conditions such as water saturation, pH, redox conditions,...etc.

Kittilä mine in Finland (Figure 1), located in the North of Finland (in central Finnish Lapland) close to Kittilä city, is the largest strenuous gold mine in Europe at the moment. It has 7.9 million ounces of gold. In the Kittilä mine, the commercial extraction of gold has started since May 2009 with pit operation. Since November 2012, this operation has changed to underground mining whose production is expected to last until 2034 [37].

Figure 1. The Kittilä gold mine [3]

The Kittilä mine, just in 2009 diverted 97 kilograms of Ferrum, 206 kilograms of Manganesse, 4.7 kilograms of Nickel, 490 kilograms Antimony, 10.1 kilograms of Arsenic and 141 tons of sulfate ion (SO_4) into the water [3]. Since then, a pilot for recycling the water has been constructed in 2015 [38]. However, the Kittilä mine, as in many other mines in Finland, uses two natural peatlands as a buffer zone in the middle of mine and nearby Seurujoki river. After this step, the output water which is treated from mining-influenced water discharges in Seurujoki river. These two peatlands, which will be named TP-A and TP-B in this thesis, have been used at distinct time interval. For instance, the operation of TP-A started in 2010, while TP-B has been used since 2006. Theses two peatlands have distinct water properties / characteristics. Accordingly, one of these peatlands, just mines dewatering flows through it, while in the other one, the mine process water flows. Due to discrepancy in water chemical properties, the impact on peatlands would be different as well [39].

The biogeochemically and hydrologically distinct treatment of each peatland will be studied separately under same conditions such as climatic, environment and geographic. However, according to a recent research in the analysis of water quality of Seurujoki River during mine operation, the seasonal change along the river has been shown to have an impact as well. Before the intersection of mining-influenced water and the river, there was a correlation between river discharge and seasonal pattern, while this correlation after this point becomes weak to negligible. Furthermore, the treatment of mining-influenced water had significant impacts on the increasing Ntotal, SO_4-2, and Sb in Seurujoki River [40]. However, some other studies reported the chemical changes of pore water on both peatlands' peat [41][42][43][44]. Whereas there is no recent research or attention to the vegetation cover in the peatlands to show the impacts of mining-influenced water treatment process on the greenness of the peatlands.

The vegetation cover is an important phenotypic propert used in forestry, agriculture and ecology [45]. Due to the fact that study areas TP-A and TP-B are 44 ha and 17 ha, respectively [39], covering large areas, the remote sensing data have the ability to analyze the vegetation cover in both peatlands, where the potential of remote sensing technologies including satellite imaging analysis is immense as per previous studies [46][47][48].

1.1. Purpose

This thesis exploits the remote sensing data available from Landsat satellites to study the impacts of treatment operation of mining-influenced water from Kittilä mine in terms of changes in vegetation cover on the target peatlands. In essence, the goal of this study is to answer the following research questions:

1. Can the remote sensing be employed to analyze the changes of greenness treatment of peatlands?
2. What is the optimal remote sensing tool for this purpose?
3. To which extent we can ignore the climatic and environmental factors in analyzing the effects of peatlands treatments?
4. Can an estimation be inferred regarding the amount and quality of impacted water by monitoring the greenness treatments of the peatlands?

In Section 2, we will review remote sensing technology, answering research question 1 and 2. In Section 3, we detail our approach for remote sensing data acquisition and show how climatic and environmental conditions would be handled in the proposed analysis, answering research question 3. In Section 4, the amount of mining-influenced water impacts on the target peatlands will be analyzed, which answers research question 4. Finally, we will cover the advantages and disadvantages of the study method in Section 5. The overview of this process pipeline is summarized in Figure 2.

The next section will cover the role of remote sensing data on monitoring of vegetation cover in more detail. Hence, the history of satellites will be discussed, and how they can be used will be mentioned. Then, we are going to write about study area.

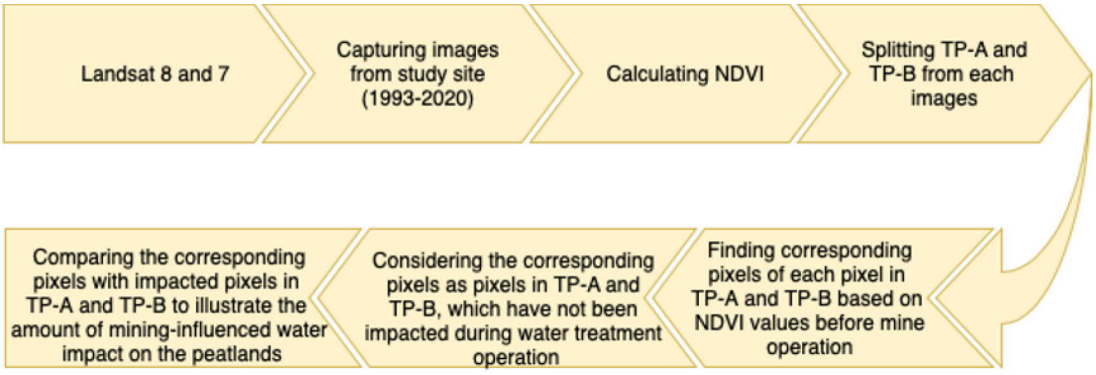

Figure 2. Process pipeline summary employed in this research

2. TOOLS AND DATA

In this study, first of all, the remote sensing data and its history of it will be explained. Then the monitoring of vegetation cover from satellite images will be discussed. Furthermore, we will talk about the study area and other practical tools for analyzing mining-influenced water.

2.1. What Is Remote Sensing Data

In general, the term of remote sensing is related to capturing data from a distance [49]. One utilization of this technique is observing Earth with satellites or aircraft, which provides the ability to detect and record the energy reflected or emitted. Accordingly, a rich dataset from such Earth's observations can be obtained to infer further decisions.

2.1.1. How to Observe Earth

The remote sensors work via electromagnetic energy (the charged iotas vibrate and produce electromagnetic energy), crossing through space and atmosphere. The electromagnetic energy is described in a wave form in different wavelengths and frequencies, that an electromagnetic with high wavelength has low frequency and vice versa. According to Figure 3, the wavelengths of x-rays and gamma rays are shorter in comparison to radio, and infrared waves, while the visible light sits almost in the middle of wavelength range.

The wavelengths of visible lights are in the range that the human eyes can recognise it and travel through atmosphere. The remote sensors observe the reflectance of Sun's energy from different surfaces and quantify amount of reflections, which depends on the surface's albedo (the ratio of reflecting energy to absorbing it) and roughness. For instance, the albedo of snow is in high level and it can reflect 90% of Sun's energy received and just 10% of it will be absorbed, while these ratios for oceans are 6% and 94%, respectively. Since the reflected part of absorbed energy has longer wavelengths, the reflected energy from the ocean is infrared radiation. The whole objects on Earth's surface can absorb and reflect energy in different wavelengths, and each object has unique wavelengths. Hence, this property gives the ability to the researchers or scientists to detect or identify objects such as rocks, water, ice, etc.

Remote sensors measure the wavelengths of reflected energy. The source of energy may be Sun or produced by a given sensor sensing the underlined object (s). Such sensors can be either active or passive depending whether thy emit energy or not. Many of passive equipment work on visible, thermal infrared, and microwave spectrum domains that measure vegetation properties and sea surface temperature.

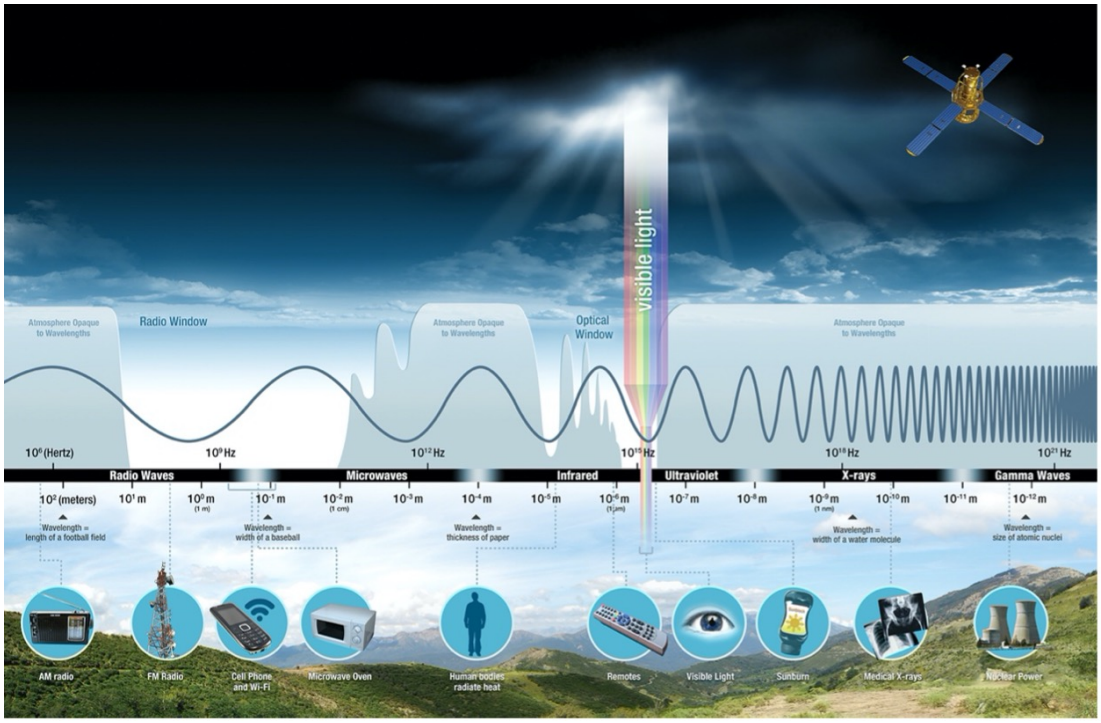

Figure 3. The wavelengths of some rays [50]

2.1.2. Landsat Satellites as a Tool to Monitor

The Landsat satellites are a series of MultiSpectral Scanner (MSS) satellites, and their key mission is to observe Earth. They are developed by NASA[2] and USGS [3]. The first mission started by Earth Resources Technology Satellite (ERTS-1), which renamed Landsat 1 later, On July 23, 1972. The mission further expanded with the launch of Landsat 2, 3, 4, 5, 6, 7 and the newest Landsat named 8 (Table 4), which was launched on February 11, 2013. While Landsat 7 and 8 orbit and collect the data, the observing Earth expects to continue with Landsat 9, which will launch in the middle of 2021.

The ground resolution of all Landsat series spectral bands is optimal, making them effective in pursuing changes in Earth's surface or climate. With this thesis, the data will be captured from Landsat 7 and 8. Also, the information of their bands is summarized in Table 5. The wavelengths of these bands ranged in the visible area.

Landsat 7 is equipped with the Enhanced Thematic Mapper (ETM+) sensor, and since 2003, gaps occurred in captured data due to the Scan Line Corrector (SLC) error. The rotation of Landsat 7 is around Earth in a near-polar and sun-synchronous circuit, with a distance of 705 km from Earth. This satellite orbits every 99 minutes, and the cycle repetition is 16 days and whose equatorial crossing time is 10:00 a.m. +/- 15 minutes. The Landsat 8 is equipped with Operational Land Imager (OLI) and the Thermal Infrared Sensor (TIRS). The rotation of Landsat 8 is around Earth in a near-

[2]National Aeronautics and Space Administration
[3]U.S. Geological Survey

Table 4. The information of Landsat satellites' launch

Satellite	Launch data	End date of mission
Landsat 1	23.07.1972	06.01.1978
Landsat 2	22.01.1975	25.0.1982
Landsat 3	5.03.1978	31.03.1983
Landsat 4	16.07.1982	14.09.1993
Landsat 5	01.03.1984	05.06.2013
Landsat 6[4]	05.10.1993	05.10.1993
Landsat 7	15.04.1999	Still orbits and collects data
Landsat 8	11.02.2013	Still orbits and collects data

Table 5. The description of Landsat 7, and 8

Satellite	Band's name	Wavelength (mm)	Resolution(m)
Landsat 7	Band 1	0.45 - 0.52	30
	Band 2	0.52 - 0.60	30
	Band 3	0.63 - 0.69	30
	Band 4	0.77 - 0.90	30
	Band 5	1.55 - 1.75	30
	Band 6	10.40 - 12.50	60
	Band 7	2.08 - 2.35	30
	Band 8	0.52 - 0.90	15
Landsat 8	Band 1	0.43 - 0.45	30
	Band 2	0.450 - 0.51	30
	Band 3	0.53 - 0.59	30
	Band 4	0.64 - 0.67	30
	Band 5	0.85 - 0.88	30
	Band 6	1.57 - 1.65	30
	Band 7	2.11 - 2.29	30
	Band 8	0.50 - 0.68	15
	Band 9	1.36 - 1.38	30

polar and sun-synchronous circuit, with a distance of 705 km from Earth. This satellite orbits every 99 minutes, and the cycle repetition is 16 days, whose equatorial crossing time is 10:00 a.m. +/- 15 minutes.

2.1.3. Spectral Indices as Tools to Monitor Vegetation Cover

Some indices have been developed for estimating the vegetation cover via remote sensing. The ratio of the wave with wavelength 800 μm to 675 μm, which is named SR or RVI, can specify the measurement of the leaf—area index of a forest [51]. In 2000 a method developed based on an index to make Leaf Area Index (LAI) better via the potential of the shortwave infrared (SWIR) signal [52]. Furthermore, during recent decades, many vegetation indices have been developed such as MSR [53], DVI [54], NDVI [55], NDVIc [56], GNDVI [57], RDVI [58], IPVI [59], CI [60], etc. Though

[6]The failed launch

there is a wide variety of spectral indices for estimating the vegetation assessment via satellite data, Normalized Difference Vegetation Index or NDVI, due to its ability to calculate via different sensors of visible and near-IR band, is the most commonly employed [61].

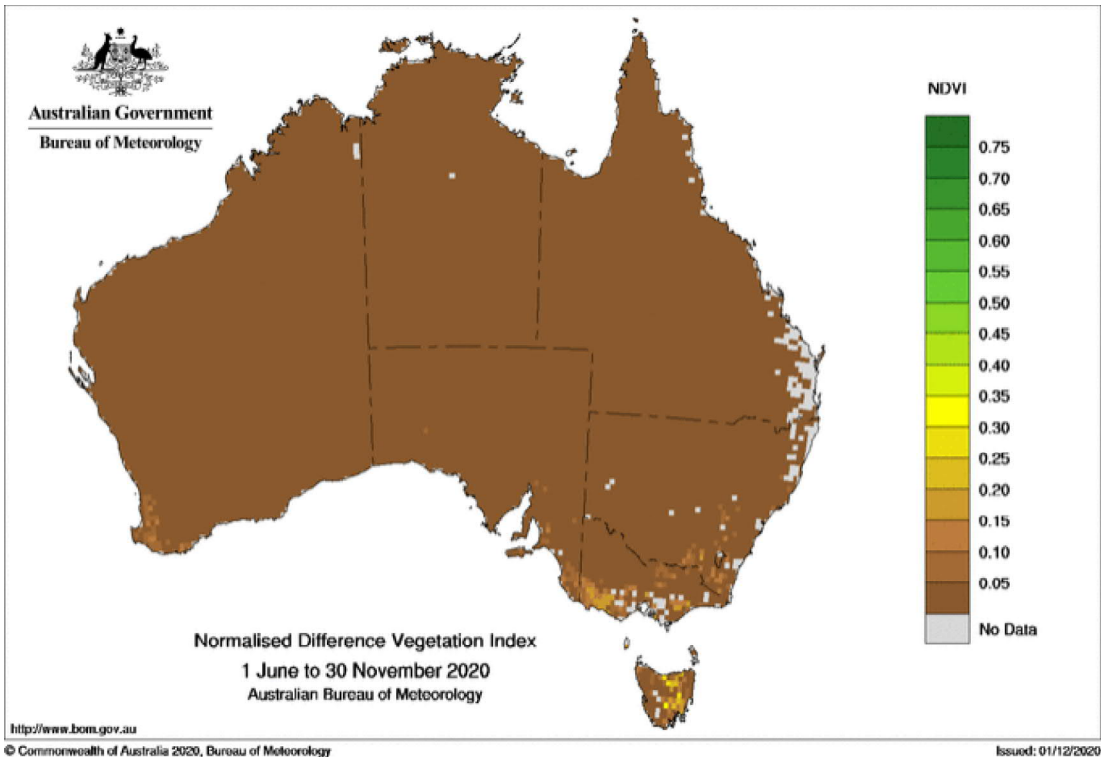

Figure 4. 6-months mean of NDVI magnitudes for Australia

After launching Landsat 1, the monitoring operation of Earth based on MultiSpectral Scanner (MSS) of Landsat 1 has started. One of the key capabilities of Landsat 1 was auscultating vegetation colour in spring, summer, and fall throughout Great Plains, which is located in the centre of the USA. A PhD student, Donald Deering, and his advisor, Dr Robert Hass, studied Great Plains through Landsat 1 and found the correlation of the vegetation biophysical characteristics with spectral signals of the satellite. With the cooperation of Dr John Schell, they found a way to show the mathematical equation of the difference of the red and infrared radiance reflection through Great Plains and called it Vegetation Index. Since then, the first introduction of Normalized difference vegetation index or NDVI was established in Great Plains study [55]. Indeed, NDVI has been utilized to analyze the vegetation cover through multispectral remote sensing data and was one of the simple and quick ways to recognize vegetation areas and their situations. These features of the NDVI index promoted the latter to be a good candidate for straightforwardly analyzing large scale areas. For example, NDVI distribution of Australia can be found in the government website[5] such as Figure 4.

[5] http://www.bom.gov.au/jsp/awap/ndvi/archive.jsp?colour=colour&map=ndviave&year=2020&month=11&period=6month&area=nat

2.1.4. How the Visible Waves Help to Monitor Vegetation

Normalized difference vegetation index works based on the reflection of different light waves. Due to photosynthesis operation in the plants, the chlorophyll pigment in plants absorbs blue and red waves whose wavelengths are 0.45- 0.67μm, respectively and reflects green waves (Figure 5), where human eyes can see the plant as green [62][63]. Hence, the near-infrared waves are reflected by a plant. In contrast, when a plant is in a healthy mode (with much chlorophyll), the obsecration and reflection of red light and near-infrared occur. However, a diseased plant does not have such property. Therefore, NVDI calculates the ratio between the difference of red and infrared waves. This ratio would scale in the range of -1, which shows snow or ice values for NDVI, and +1, which would be the complete vegetation cover [64].

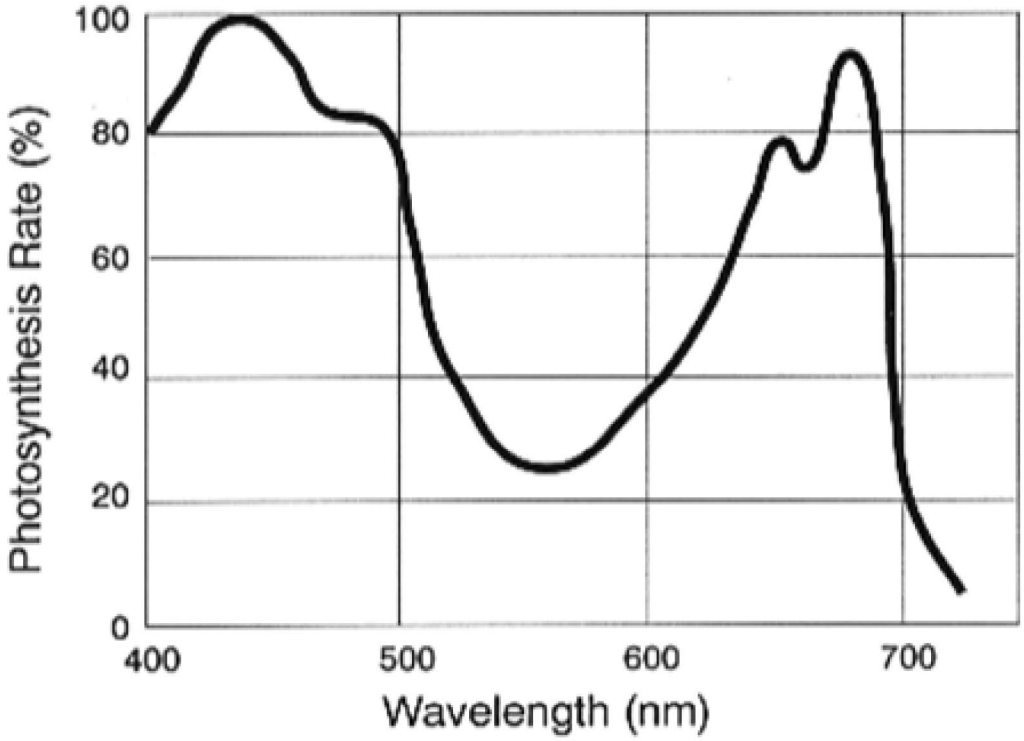

Figure 5. The wavelength range, which is absorbed with chlorophyll pigment during photosynthesis operation [65]

2.1.5. The Information behind Different Values of NDVI

According to Table 6, the NDVI magnitudes have different values in various vegetation environments such as forest, grassland, broadleaf, open shrubland, and etc.

Table 6. Examples of NDVI values based on green environments in some recent studies

Target Area	NDVI value for soil	NDVI value for live plant	Dataset	Target areas for soil and live plant	Researcher
Eastern US	0.04	0.52	AVHRR sensor	GI values	Gan and Burges, 2006 [66]
China	0.05	Grassland=0.49 Open shrubland=0.60 Mixed forest=0.68 Broadleaf and deciduous forests= 0.70	AVHRRsensor	Zeng at al., 2000 prepared values [67]	Yang and Yang, 2006 [68]
Nepal and Mexico	0.05	Open shrubland= 0.52 Mixed forest = 0.95	MODIS	Zeng at al., 2000 prepared values for open shrubland [66]	Tan et al., 2011 [69]
Global	0.04	0.52	AVHRR sensor	Desert annual for soil and evergreen annual for live plant	Gutman and Ignatov, 1998 [70]

2.1.6. How to Calculate NDVI

As mentioned before, in this study, the Normalization Difference Vegetation Index or NDVI extractes from images captured from Landsat 7 and 8. The equation of NDVI calculation is explained in Equation 1. The red and near-infrared bands for Landsat 7 are band three and band 4, respectively. For Landsat 8, this corresponds to band four and band 5, respectively. The overall band information summarized in Table 5. The output of Equation 1 shows the density of vegetation crown, whose value lies -1 and +1. More specifically, NDVI is formulated as follow:

$$NDVI = \frac{B_{near-infrared} - B_{red}}{B_{near-infrared} + B_{red}} \quad (1)$$

A normalization procedure radiance rescaling factors for calibrating of Landsat 8 data is needed [71].

2.2. Study Area

The study mine sites lie in the Northern part of Finland, with the geographical location of 67°54'N; 25°22'E (more information is available in appendix). The passive treatment of output mining-influenced water of this mine has been done through two peatlands, called TP-A and TP-B as in Figure 6, while the treated water goes to Seurujoki river. The polishing treatment as pre-treated is provided via

TP-A, while the pre-treated mining-influenced water is handled at TP-B. Usages of TP-B and TP-Ahave started in 2010 and 2006, respectively. Due to environmental issues, the mining company is responsible for taking the required steps to comply with the water quality requirements before allowing wastewater into the peatlands. Khan et al. (2020) has performed a complete research on the chemical composition of water discharged into TP-A and TP-B. Through other polluters in the mining-influenced waters, which flow in both peatlands, the amount of sulfate shows to be relatively high. However, sulfate concentration in TP-A is more than that of TP-B. The extra sulfate concentration led to the implementation of an extra plant that has been used since 2017 for treating operation in terms of sulfate reduction through PT-A.

The region category of the study area is Dfc (snow climate characterized by moist, cold winters) is categorized in a climate classification system, known as Köppen [72] [73]. The winter in this environment commonly starts from October until May, where the average temperature is lower than 0 °C, and the snow cover is almost available throughout the whole winter (according to the Finnish meteorological institute). This area has a flat topography, and the annual amount of precipitation is 197 mm on average.

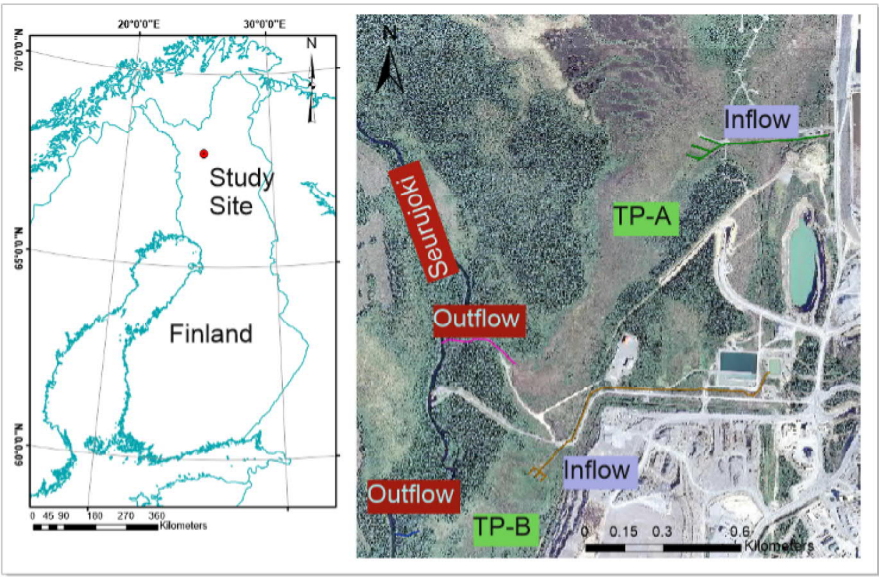

Figure 6. The places of gold mine, TP-A and TP-B

The estimation of NDVI value without wastewater will be discussed, and then the operation of making the method faster will be explained in more detail.

3. IMPLEMENTATION OF PROPOSED TECHNIQUES

In this section, the capturing data process from target satellites will be covered. Then the methods of estimating the impacts of mining-influenced water on the target peatlands will be explained. Then the innovative way of speeding data mining would be detailed.

3.1. Capturing Images Process

The Tier 1 composite NDVI images used in this study were captured from Landsat 7 from 1993 until 2012 and Landsat 8 between 2013 and 2020. However, data taken from Landsat 7 has gaps since May 31, 2003, due to failing of Scan Line Corrector (SLC). This sensor is responsible for restituting for the forward movement of Landsat 7. The operations for recovering SLC were not successful, and this error is still available. When SLC does not work, the sightline of the sensor pursues a zig-zag pattern. In contrast, the images were useful until 2005; after that, until 2012 there were not applicable.

From 1993 until 2020, 290 Tier 1 composite NDVI images extracted and 93 out of them owned before operation (`https://developers.google.com/earth-engine/datasets/catalog/LANDSAT_LC08_C01_T1_8DAY_NDVI?hl=en`). The consideration of capturing images was an 8-day period and the infrared and red bands in each scene were considered to calculate NDVI magnitudes. The script for capturing images, which were used in this study, as defined on Google Earth Engine(GEE[6])

[6] `https://code.earthengine.google.com`

3.2. Vegetation Cover Difference in TP-Aand TP-B, with and without Mining-Influenced Water Impacts

The Normalize Difference Vegetation Index or NDVI of each pixel of remote sensing captured images from TP-A and TP-B have two different values, one of them is a NDVI magnitude, which is affected via mining-influenced, and the other stands for the NDVI amount, which is not affected during water treatment operation. The first NDVI magnitude impacted with treatment operation is calculated directly from remote sensing captured images. However, the most challenging issue in this study is the estimation of the NDVI magnitudes of TP-A and TP-B without mining-influenced water impact. Statistical methods may predict the NDVI values, but the most challenging problem is environmental changes, which would not be predictable, such as temperature, precipitation, the amount of solar radiation. In addition, the difference between two different NDVI values, which are approached without and with mining-influenced water, expresses the amount of vegetation lack that has been produced during the mining operation. Therefore, the main question is how to present this difference?

In mathematical science, for approaching the difference between two quantities, the relative change and the relative difference are used, and this difference commonly is expressed as a percentage (a ratio multiplied by 100), which is a unitless number. The assessment between "change" and "difference" based on which one assumes as standard, reference or starting quantity. Common usage of Relative Difference of RC is a factor for showing quality control. The actual difference between a and b, two quantities, is represented with Δ.

If there is no issue which number should be a reference and cited in the first place, Δ has little meaning, and the absolute difference is using such as $|\Delta|$. When $|\Delta|$ shows the actual change, where the compared value would be larger or smaller than the reference value, comparing that which of them is bigger or not is not necessary. Though, the absolute difference is not a comparing way, which would be good anywhere. For instance, the difference between 211,788,999 and 211,788,998 is not significant as same as diversity between 3 and 4. Since taking into account the “size” operation would be a good way such as Equation 2, where values of $a_{reference}$ are positive.

$$RelativeChange(b, a_{reference}) = \frac{b - a_{reference}}{a_{reference}} \tag{2}$$

When $a_{reference}$ =0, the Equation 2 cannot be defined.

After all, the expression of value changes of a quantity would be represented via percentage change of two different values. According to the defined issue of this study, which is estimating of NDVI values of each pixel in TP-A and TP-B without impacts of mining-influence water, the new value of NDVI of each pixel will be prediction NDVI value, and the old value is real NDVI computation under mining-influence water impact of each pixel in target areas. The estimation value will show as $NDVI_{el}$ and the

real value would represent as $NDVI_{il}$. The change value between $NDVI_{el}$ and $NDVI_{il}$ would be expressed via percentage change as Equation 3:

$$RC = \frac{NDVI_{el} - NDVI_{il}}{NDVI_{el}} \times 100 \tag{3}$$

3.3. Estimation of NDVI Values without Mining-Influenced Water Impacts

The main issue mentioned before and the main target of this study is how to predict NDVI value of each pixel in captured remote sensing data without mining-influenced water effects via considering the same environment changes such as temperature precipitation, etc. For estimating of $NDVI_{el}$, a linear regression coefficient was employed, and with this method, it has tried to approach a correct prediction of NDVI as the same temperature, precipitation, etc., which were available when the real NDVI through water treatment operation has been calculated.

Henceforward, the strategy of this method is finding pixels, which place outside of TP-A and TP-B, that have the highest correlation with the pixels in both target areas. Thence, these pixels are named pair pixels, and their NDVI magnitudes are considered as $NDVI_{el}$ during the mining operation. Therefore, this technique gives the ability to this study to find pixels that have the same patterns of NDVI value changes before mine extraction with pixels in TP-A and TP-B, to come up with a prediction of NDVI without water treatment operation impacts without considering environmental conditions such as temperature, precipitation, etc. And the environmental effects will be removed from the prediction due to the pair pixels and pixels in target environments faced or will experience the same conditions, which are created naturally.

For finding the outside closest pixels with target areas' pixels, detecting the highest correlation before mine operation is necessary. Accordingly, the correlation is a uniform association between two variables, so applying a method to find the correlation coefficients will be necessary. The relationship between two variables is defining in this way if one variable follows an increasing pattern, another increase, but in another way, if one of them raises the other, one decrease. When magnitudes of a quantity increases and the correlated quantity rise, in this situation, the correlation is positive, otherwise it decreases the correlation is negative. The correlation between 2 magnitudes, which can be continuous, random variables, etc., is known as Pearson correlation. In addition, when r equals zero means there no correlation between two variables. On another side, when the relationship becomes stronger, r is going to be 1 or -1 [74].

The relationship was categorized into "strong", "moderate", and "weak" according to the coefficient; for instance, the correlation with a coefficient of 0 - 0.39, 0.4 – 0.69, or 0.7 – 1 is supposed as a weak, moderate, or strong relationship. When there is no essential interpretation, the square of the correlation coefficient or R^2 could be used, which is called the coefficient of determination. This coefficient will show the variance of a variable, which is enumerated by another variable. Due to the R^2 is always positive and never cannot be negative, the information about the direction of correlation is not available anymore [74].

As mentioned before, the main idea of this study is finding the pare pixels of pixels in target areas' captured satellite images, which are called TP-A and TP-B, and during mine gold operation, the NDVI values of these pixels are considered as $NDVI_{el}$. For finding the pare pixels in the outside environment and their corresponding pixels in study areas, the almost same NDVI changes should be followed before the operation

of gold extraction. Hence, the highest Pearson coefficients are calculated for each pixel in target zones, and all available pixels in the outside environment and, and the highest computed correlation coefficient will be found.

3.4. Employing Pearson Coefficient

Pearson Coefficient is defined by the covariance of two quantities, and it is divided by the output of the product of the variables' standard deviation as the following equation (Equation 4). Furthermore, this equation gives a value between -1 and +1.

$$r_{i,o} = \frac{cov(i,o)}{\sigma_i \times \sigma_o} \tag{4}$$

If 'i' is a pixel in one of the study areas and 'o' is a pixel located outside of those environments, then $r_{i,o}$ is the correlation coefficient between 'i' and 'o', cov(i,o) is the covariance of 'i' and 'o', σ_i and σ_o are standard deviations of 'i' and 'o' respectively.

$$cov(i,o) = mean[(i - mean[i]) \times (o - mean[o])] = mean[i \times o] - mean[i] \times mean[o] \tag{5}$$

While the 'i' and 'o' are a set of NDVI values, which were captured before mine extraction, then they are vectors of NDVI magnitudes.

$$\begin{aligned} \sigma_i &= \sqrt{\tfrac{1}{n} \times \textstyle\sum_{m=1}^{n} (i_m - \mu_i)} \\ Where \quad \mu_i &= \tfrac{1}{n} \times \textstyle\sum_{m=1}^{n} i_m \end{aligned} \tag{6}$$

The Equation 6 explains the standard deviation of 'i', and the same operation would be done for 'o'.

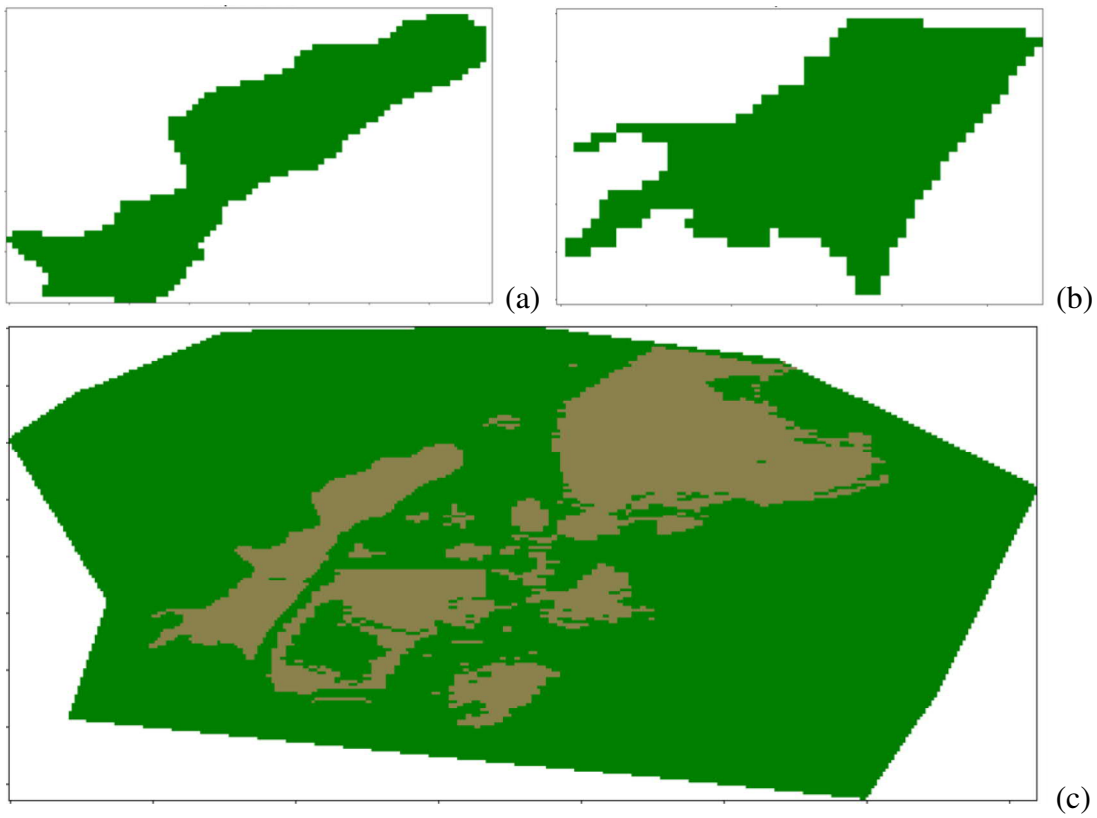

Figure 7. NDVI map is shown as green, and the unevaluable pixels are shown as brown. (a) TP-A shape, which is separated from the main image; (b) TP-B shape, which is separated from the main image; (c) Outside area, which will be mined pare pixels

3.5. How to Increase the Speed Correlation Mining Operation

Another challenge in this study is the speed of searching for finding corresponding pixels. In this study, three datasets have been approached via separating TP-A and TP-B from the whole image, so the rest part remains as an outside environment. The datasets are being seen in Figure 7. However, after separating the TP-A, TP-B, and surrounding area images contain 49, 31 and 166 rows and 81, 57 and 360 columns, respectively. In another way, these images have 3,969, 1,767 and 59,760 pixels. Each pixel has a NDVI magnitude from -1 to +1, so the pixels have three dimensions: width, height coordinates, and NDVI value. In addition, each pixel can be represented as (x,y,d), where x, y are the width and height coordinates of that pixel in the images, and they vary from width and height of the image, while d shows the NDVI value, it changes based on the date, that the images are captured.

Figure 7 (a), (b) and (c) include 49, 31 and 166 rows and 81, 57 and 360 columns respectively. Each NDVI index that belongs to each pixel has been introduced with three dimensions (x,y,d) which x and y are the width and height coordinates of that pixel in the images, and d is the date of NDVI magnitude, which was captured. For instance, if n images would be available before mine operation, d would have n different values, which means each pixel is a vector of n magnitudes of NDVI. In this study, there are 98 remote sensing images, and d will have NDVI from them. The

main goal of this study is to find the highest correlation between pixels in TP-A and TP-B with the surrounding environment before the mine operation. In this mining, there are some search operations.

The first search belongs to finding all pixels' NDVI values. For example, 98 remote sensing images, so each pixel in TP-A, TP-B, and outside environment has 98 NDVI magnitude, and all of them must be found. Then the next search and third search are related to search in rows and columns of TP-A and TP-B, in continuing the fourth and fifth search is in surrounding image's rows and columns. Generally, there are two different five searches, and for finding the pares of pixels in TP-A, $49\times81\times166\times360\times98$ finding Pearson Coefficient are necessary this number for TP-B is $31\times57\times166\times360\times98$.

In a computer programming environment, this execution is implementing two five loops, which are nested loops. The complexity of it will be the degree of five or $O(n^5)$, where 'n' is the notation of O. In other words, where n^2 iterations will be needed. This complexity, such as implementation, would increase the cost, running time, and storages (Wilf, 1994). For example, each finding Pearson Coefficient operation via Python 3 in a system, which includes an i5 processor, took approximately 3 seconds, and for $49\times81\times166\times360\times98 + 31\times57\times166\times360\times98$ will be a huge time, that this process will take.

As mentioned before, the complexity of an algorithm or mining makes issues such as time running increase, memory usage raising, etc. Hence, introducing a complexity reduction method will be necessary. There are some models of computation to reduce the complexity of computer algorithms, such as sorting, searching, etc., which will be mentioned in the following:

1. **Deterministic**: The performed machine and activities, which are successive states, determine this model as a state that is preceded, such as lambda calculus, recursive functions, etc.
2. Non-deterministic: this model will make some choices in some calculation steps.
3. **Parallel and distributed calculation**: In this model, many processors or machines execute one operation simultaneously. Hence, a big operation could be distributed or divided into small operations, and each operation would be done in a separate processor. There is a range of parallel computations such as bit-level, data, task parallelism, and instruction-level.
4. **Quantum processing**: In this computing, the whole operation will be done in a quantum system.

While the complexity of an algorithm will be decreased via reducing the degree of 'n' in $O(n^m)$, in other words, the main target would be the decrease of 'm'. There are several methods to decrease 'm', that one of them could be loading all data as input since this is the idea that will be represented as an innovative way to reduce the time-consuming of the introduced mining data in this study.

The new technique will decrease the searching and create a matrix with two dimensions, row and column, for each dataset from three datasets (TP-A, TP-B and

surrounding environment). The supposed goal is limiting the search operation in rows of matrices. Hence, each row includes a single pixel with whole NDVI magnitudes before mine operation, wherein this study has 98 captured remote sensing images, so the number of columns of each matrix is 98. The row index of each matrix demonstrates the x and y coordinates of a pixel. In this way, the divisor and reminder of division operation of the row over the target image's width will produce y and x coordinates of the pixel such as Equation 7:

$$y = \left\lfloor \frac{row - index}{image'swidth} \right\rfloor \quad and \quad x = (row - index)\%image'swidth \tag{7}$$

If the above technique were implemented on the three datasets, the final output would include three matrices with 3,969, 1,767 and 59,760 rows, and all of them have 98 columns for TP-A, TP-B and surrounding area, respectively, as shown in Figure 8. Since the complexity of this technique will be O(N^2), two loops will be necessary, one for TP-A or TP-B and another for the surrounding environment matrix. For instance, for finding the highest correlation of each pixel in PT-A with the outside environment, a loop for reading 3,969 rows and another for reading 59,760 rows will be essential.

All in all, after creating an optimum searching in the final operation, the Pearson Correlation and p-value of each pixel in PT-A and PT-B with whole pixels in the outside zone will be calculated with the condition, where the Pearson Correlation and p-value should be more significant and lower two thresholds of 0.8 and 0.05. Then the highest pares that has a strong correlation will be determined and stored. The pseudo-code is explained in Algorithm 1 entirely (The python code is available in the appendix).

Algorithm 1 How to fine the pare highest correlation

```
Targets ← Reshape(Target − Area);
Outsides ← (Outside − Area);
for Target in Targets do
    for Outside in Outsides do
        if Correlation(Target, Outside) > 0,8 and p−value(Target, Outside) < 0,05 then
            if Correlation(Target, Outside) > Max and p − value(Target, Outside) < Min then
                get(indexofTargetandOutside);
            end if
        end if
    end for
end for
return Created − New − Dataset − With − Index − of − Outsides;
```

In Algorithm 1, first of all, each image with m rows and n columns of one of the study areas, which could be TP-A or TP-B, and outside environment before mine operation will be reshaped as one column and then will be added to the target matrices such as the following operation.

Column 1 = [date 1,$pixel_{1,1}$,$pixle_{1,2}$, . . . ,$pixel_{1,n}$, . . . ,$pixel_{m,1}$,$pixel_{m,2}$, . . . ,$pixel_{m,n}$]^T
Column 2 = [date 1,$pixel_{1,1}$,$pixle_{1,2}$, . . . ,$pixel_{1,n}$, . . . ,$pixel_{m,1}$,$pixel_{m,2}$, . . . ,$pixel_{m,n}$]^T
.
.
.
Column k = [date 1,$pixel_{1,1}$,$pixle_{1,2}$, . . . ,$pixel_{1,n}$, . . . ,$pixel_{m,1}$,$pixel_{m,2}$, . . . ,$pixel_{m,n}$]^T
Matrix = [(Column 1)^T,(Column 2)^T, . . . , (Column K)^T]

Matrix has two dimensions, which the size of rows is equal to the number of pixels of the image, and the columns are equal to the number of captured images. This operation will be done for TP-A, TP-B and outside environment, and after that, the searching operation for pare pixels will be done between the Matrix of TP-A and outside environment, and TP-B and outside environment. After finding the pare pixels, two new datasets will be created that contains the pare pixels of pixels in TP-A and TP-B. After that, we reshape the matrix index of each couple of pixels and find the coordinates of them in target images. For example, the pare pixels outside will be determined, and their corresponding will be determined in TP-A and TP-B.

Reconstructing the row index of each vector in each matrix will be divided over the width of the image and its divisor, and a reminder will be considered as y and x coordinates in the image. Thus, for example, each row of TP-A's matrix will be divided to 81, while for the surrounding environment's matrix, this number is 360, and for TP-B is 57.

In the next chapter, we will analyze the output of the introduced techniques. First of all, the months, which have more chance of having a high level of NDVI, will be recognized. Then, the impacts of mining-influenced water's treatment on TP-A and TP-B will be analyzed in more detail.

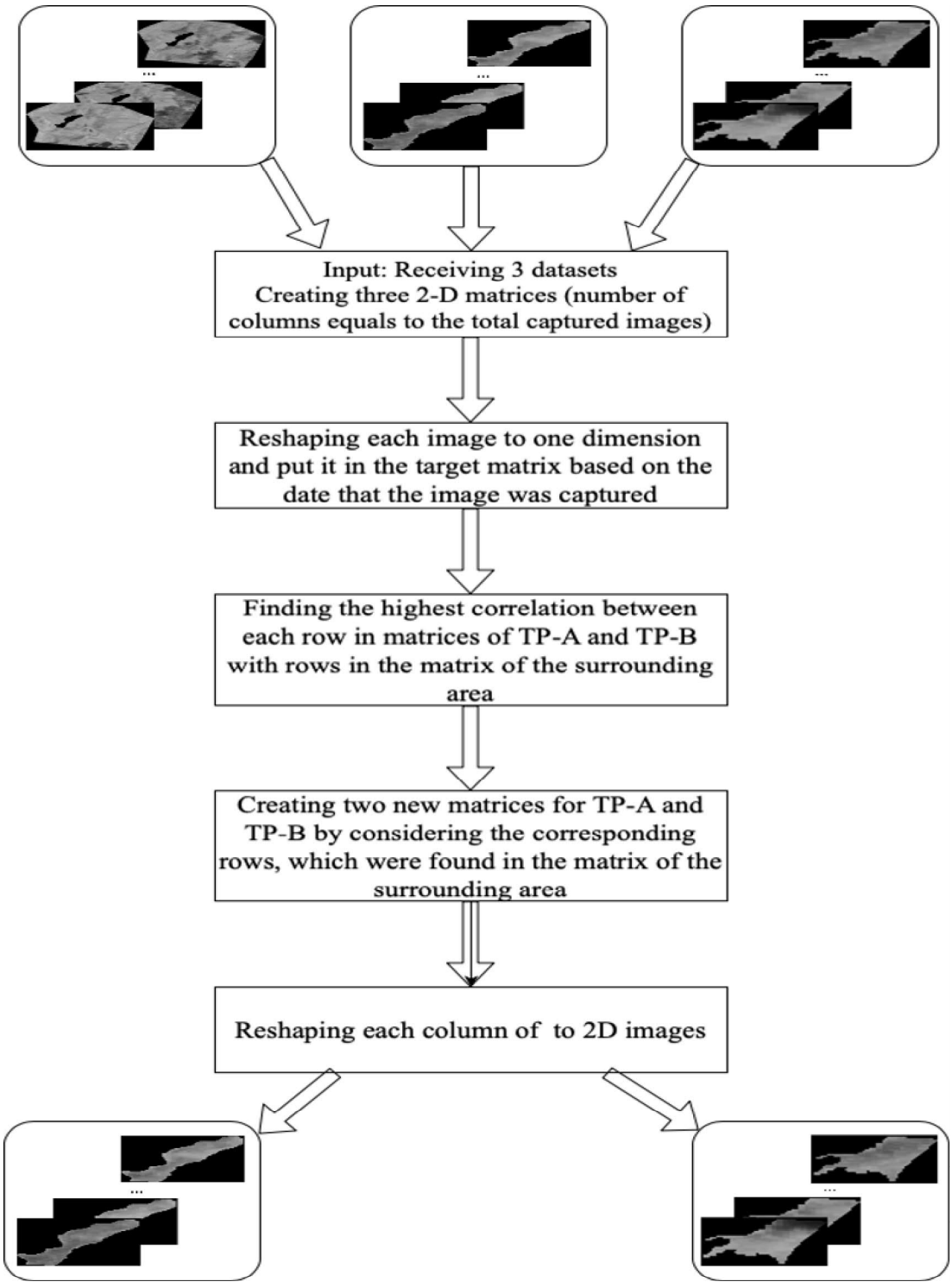

Figure 8. The steps, which will be done to identify the mining highest correlation in this study

4. EXPERIMENT AND RESULT

4.1. The Changes of NDVI Magnitudes Based on Months

The first thing, which should be done, is defining the trend of NDVI value changes during the time and clarifying the factors that impact NDVI magnitude. Hence, Piao et al., 2003, has researched this trend. Accordingly, there is a connection of NDVI trends with climate changes based on three seasons of autumn, summer and spring and human activity in their research. In that research via analyzing remote sensing data, which was captured from North of China between 1982 and 1999, they found when there was a NDVI raising based on months and seasons at the scales, which are national and biome, so they showed the impacts of climate changes on trend pattern of NDVI magnitudes. In more detail, based on national scale analysis, when the mean temperature was increasing in spring, summer and autumn, the mean NDVI raised significantly.

Moreover, this relationship was also between NDVI and precipitation. On another side, there were impacts of human operations such as agriculture and citification activities on NDVI trends in some areas such as Yangtze River and Pearl River deltas, and urbanization process, which was happened in a short time, NDVI magnitudes declined [75].

Equally, in another research via monitoring monthly changes of NDVI in the Northeast part of China between 1982 and 2009 (the remote sensing images were captured from MODIS and AVHRR), there was a relationship between NDVI trends and patterns of climate changes. During the 28 years, the monthly NDVI changed based on climate properties in different seasons [76].

In this study, the monthly NDVI values would be analyzed during the 13 years before mining and water treatment operations. As a result, the annual mean NDVI magnitudes based on moths in TP-A and TP-B had changed. In more specific, according to Figures 9 and 10, the trend of NDVI changes in both target areas before water treatment operation correlates with monthly climatic variables and based on months, it changed.

All in all, the exact information would be extracted from Figures 8 and 9; there was not a significant vegetation cover in both areas in March, and in this month, TP-A and TP-B were almost bare, which included a few pixels (lower than about 5% of whole pixels) with NDVI values more than 0.06(section (a) in Figures 9 and 10). Furthermore, the distributions of NDVI in March through both zones varied between 0.02 and 0.04, which might mean these areas were covered with snow or ice, and the information about water treatment impacts on vegetation cover will not be extracted.

In continues, by looking at the distributions of both target areas in April (section (b) in Figures 9 and 10), there was any progress about vegetation cover, and such as March, the most pixels of them had NDVI between 0.02 and 0.04. So, the information

about vegetation cover impacted with mining-influenced water is not clear this month also.

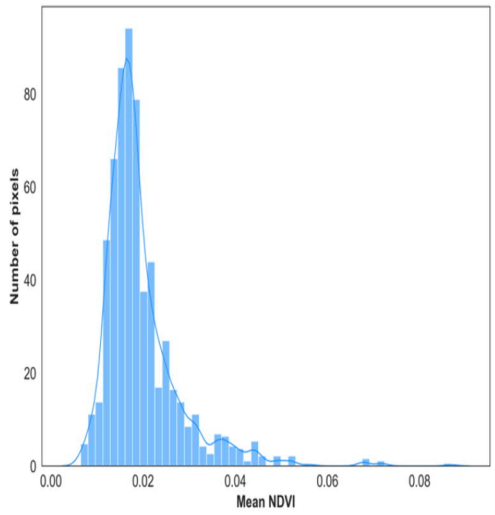
Number of pixels
Mean NDVI

(a)

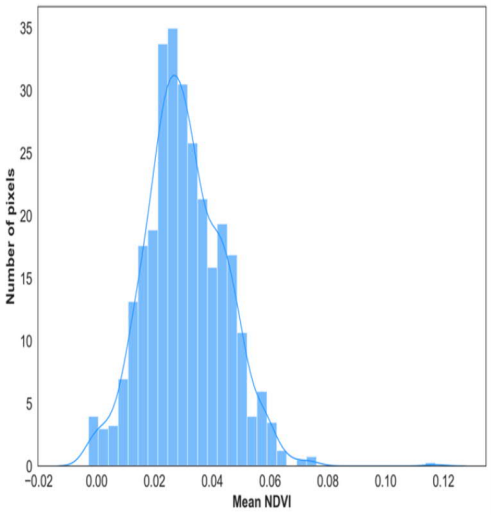
Number of pixels
Mean NDVI

(b)

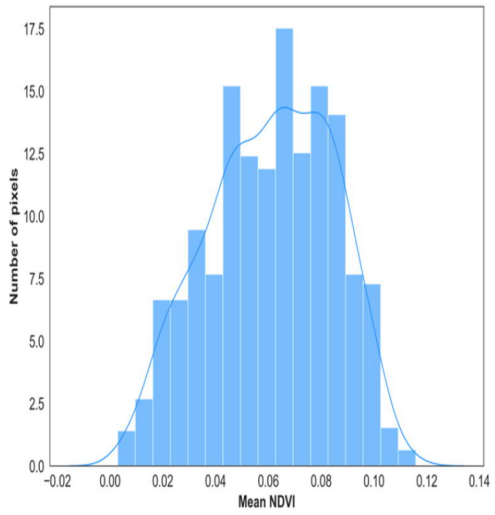
Number of pixels
Mean NDVI

(c)

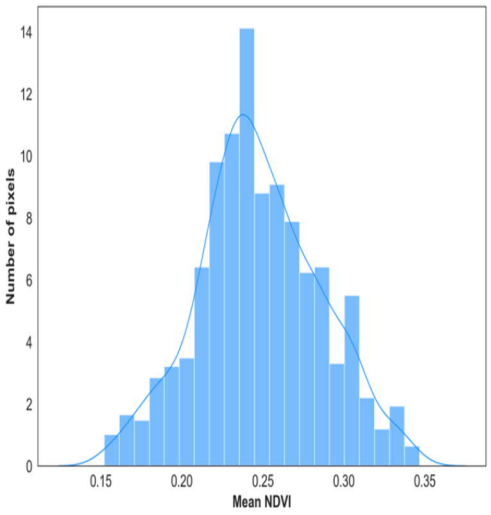
Number of pixels
Mean NDVI

(d)

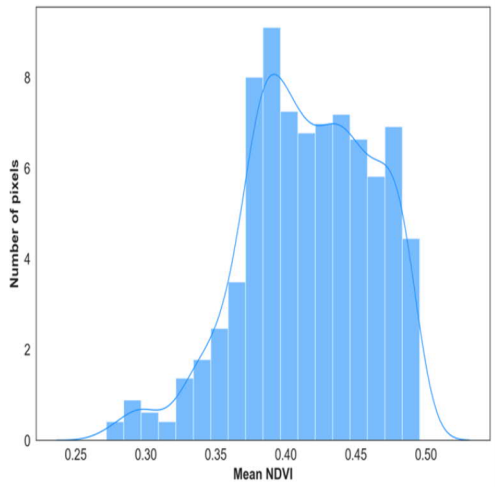
Number of pixels
Mean NDVI

(e)

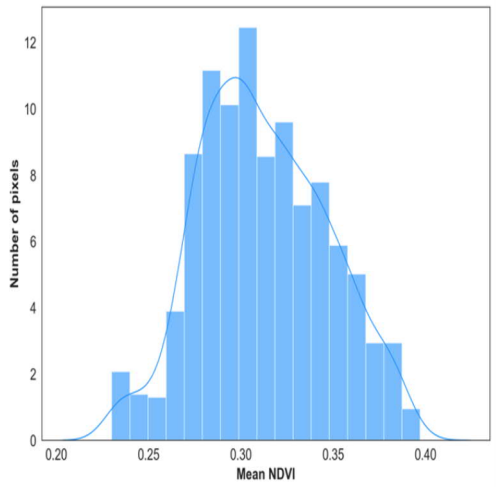
Number of pixels
Mean NDVI

(f)

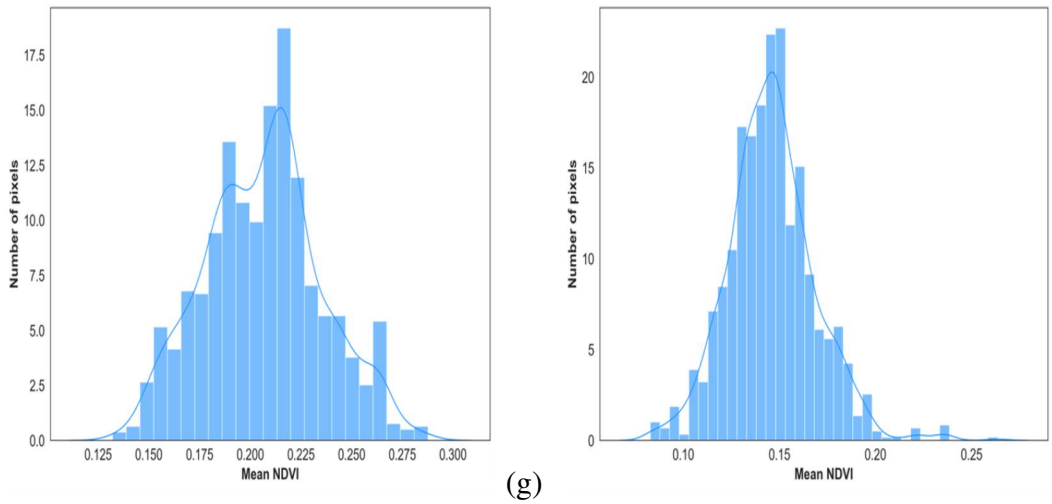

(g) (h)

Figure 9. The distribution of annual NDVI mean-value based on months before water treatment and mine operation in TP-A with the curve of density. (a) annual mean distribution in March; (b) annual mean distribution in April; (c) annual mean distribution in May; (d) annual mean distribution in June; (e) annual mean distribution in July; (f) annual mean distribution in August; (g) annual mean distribution in September; (h) annual mean distribution in October

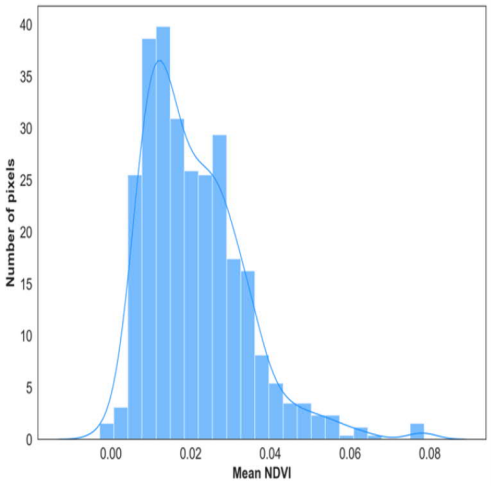
Number of pixels
Mean NDVI

(a)

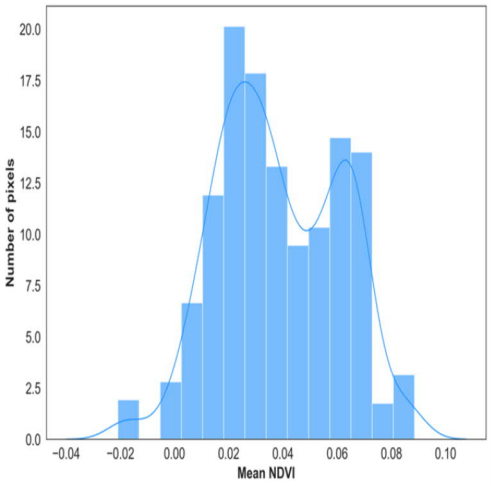
Number of pixels
Mean NDVI

(b)

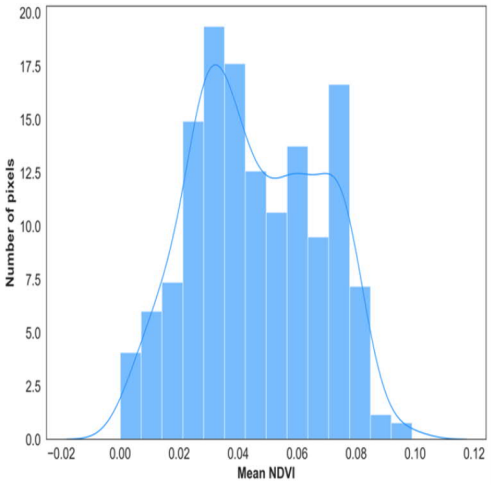
Number of pixels
Mean NDVI

(c)

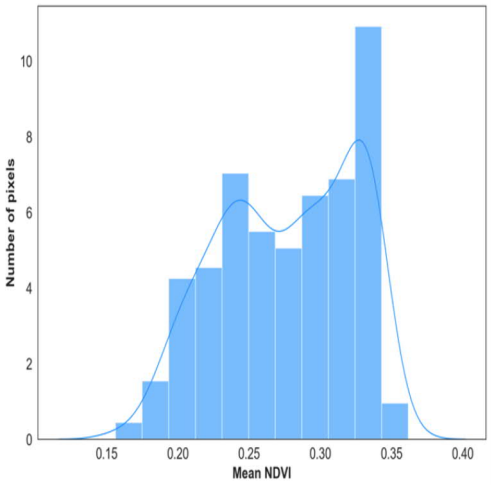
Number of pixels
Mean NDVI

(d)

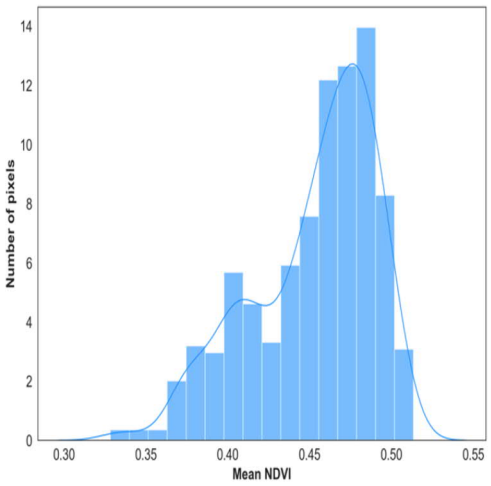
Number of pixels
Mean NDVI

(e)

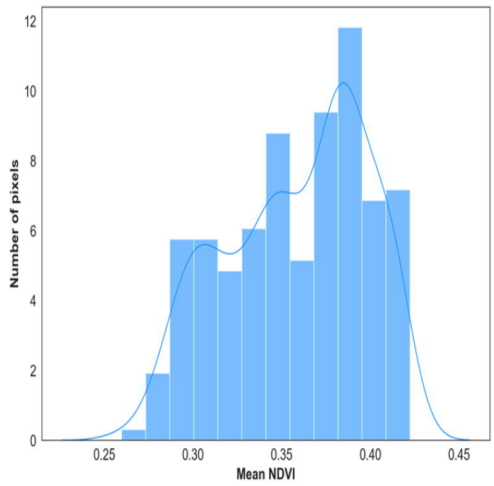
Number of pixels
Mean NDVI

(f)

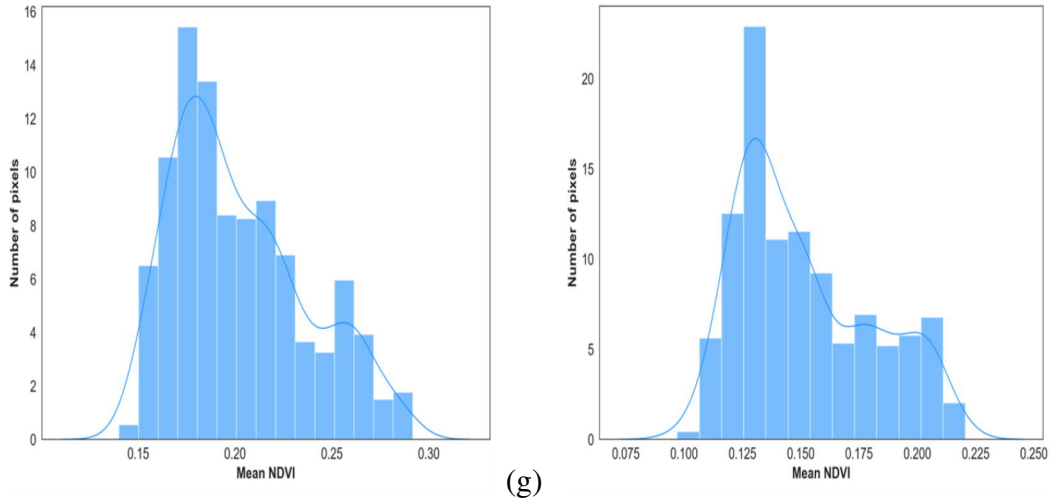

(g) (h)

Figure 10. The distribution of annual NDVI mean-value based on months before water treatment and mine operation in TP-B with the curve of density. (a) annual mean distribution in March; (b) annual mean distribution in April; (c) annual mean distribution in May; (d) annual mean distribution in June; (e) annual mean distribution in July; (f) annual mean distribution in August; (g) annual mean distribution in September; (h) annual mean distribution in October

However, the status of TP-A and TP-B's vegetation cover will be better in May (section (c) in Figures 9 and 10), but still, the primary pixels had the NDVI magnitudes lower 0.1, and in this month the NDVI distribution varied through 0 and 0.1.

However, in June, the NDVI values in both environments increased, and most of the pixels have NDVI magnitudes were more than 0.2. In this month, both peatlands included the annual NDVI mean value between 0.15 and 35, and according to the curve density, the mean values are around 0.25 for both of them. All in all, this increasing trend continued in July, which the values of NDVI approached even 0.5, which is a considerable amount. In addition, there was a bit of NDVI declaration in August, and the max amount of annual mean value of NDVI gained 0.45. After August, the NDVI situation of green cover in TP-A and TP-B started to decrease. In September, the NDVI magnitudes decreased, and in October, this trend continued. Moreover, for extracting more information, the Mann-Kendall[7] trend test has been done on the target peatlands, which shows the trend of the mean value of whole pixels increased in TP-A and TP-B from March until July, while this trend decreased for the average value of absolute NDVI values between July and October in the target peatlands. The results of the Mann-Kendall trend test are available in Table 7.

[7]More information about this test is available in appendix

Table 7. Mann-Kendall trend test results

Area	Period	p-value	slopes
TP-A	March-July	0.012	0.023
	July-October	0.012	-0.095
TP-B	March-July	0.012	0.017
	July-October	0.012	-0.095

4.2. Testing the Proposed Method for Estimating NDVI Values without Mining-Influenced Water Impacts

To ensure the proposed method's accuracy, a test has been done. In this test, from the surrounding area, three pixels were chosen randomly. First of all, with the Pearson coefficient, it was tried to find the pixels, which have the highest correlation with them based on captured NDVI values before the mine operation. Then, during the mine processing, the actual amount of the chosen pixel was compared to the NDVI values of their pares. In this experiment, these pixels, located in the surrounding, have not impacted with mining-influenced water effects, and they should have the same NDVI values with their corresponding pixels when the mined gold has been extracted.

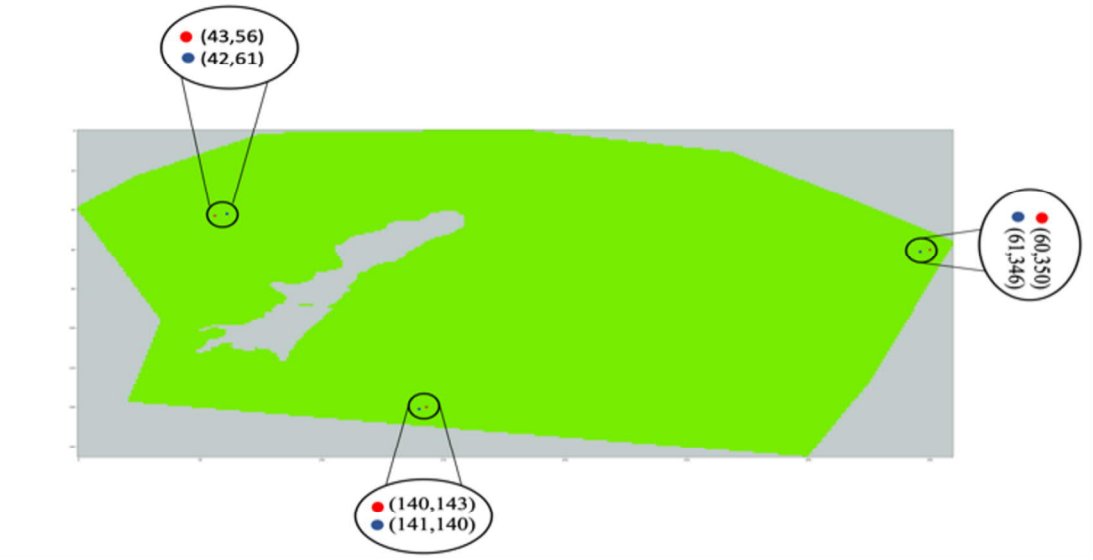
(43,56)
(42,61)
(60,350)
(61,346)
(140,143)
(141,140)

(a)

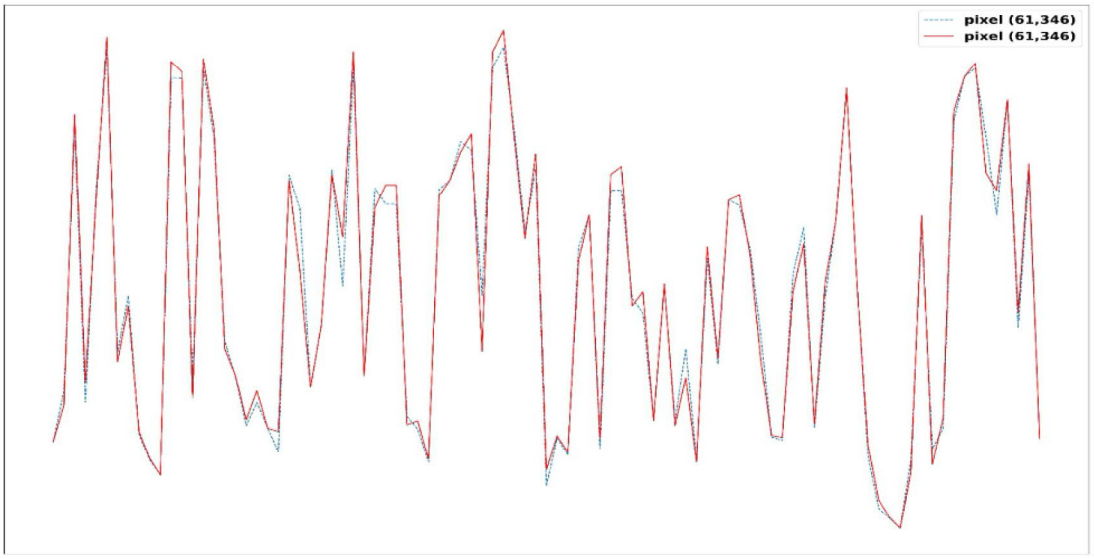
pixel (61,346)
pixel (61,346)

(b)

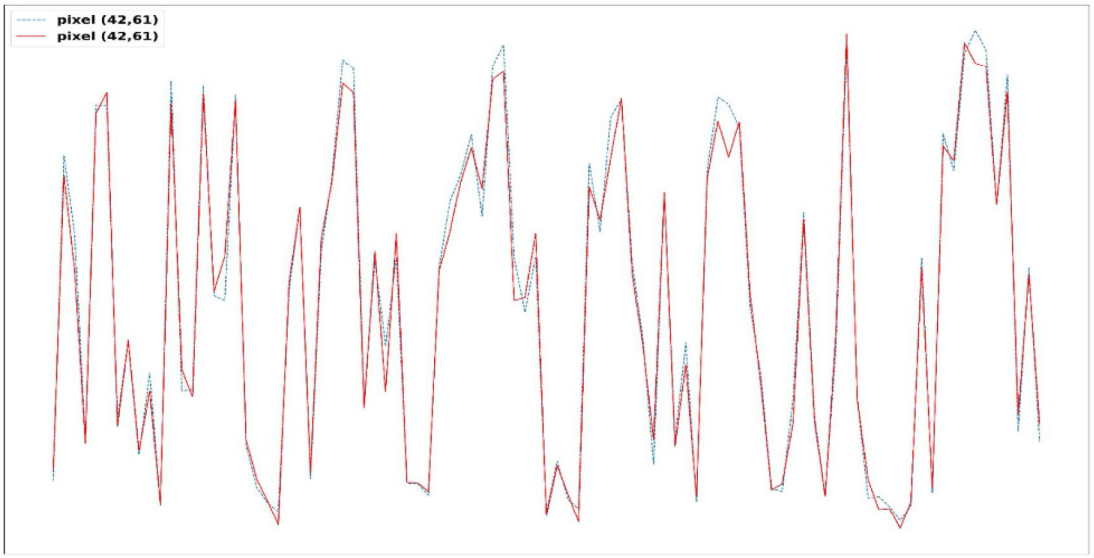
pixel (42,61)
pixel (42,61)

(c)

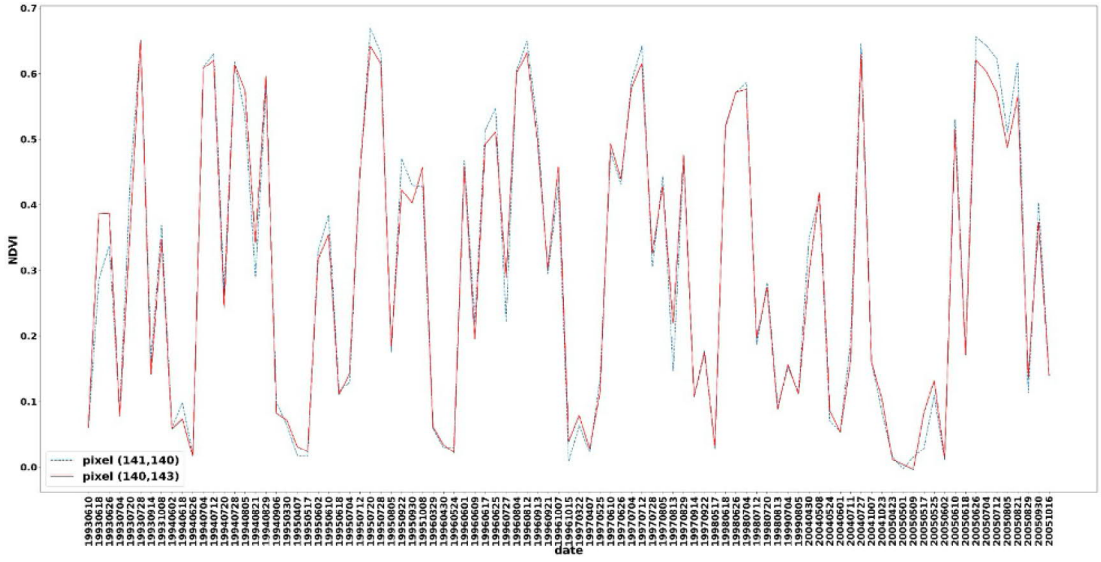

(d)

Figure 11. The NDVI values of random selected pixels before mine operation. (a) Red color is the position of randomly chosen pixels, and blue color shows the position of their corresponding pixels. (b) The NDVI values of pare pixels, where located in (61,346) and (60,350), before mine extraction. (c) The NDVI values of pare pixels, where located in (42,61) and (43,56), before mine extraction. (d) The NDVI values of pare pixels, where located in (141,140) and (140,143), before mine extraction.

Section (a) of Figure 11. shows the pixels, which were selected for the experiment randomly, and their corresponding pixels, which were obtained with highest correlation coefficient, in surrounding environment. The point of these pixels is that they have not been impacted by the output water from the mine. In this test, the corresponding pixels of chosen pixels have been obtained with NDVI values before mine operation, between 1993 and 2005,(11, section (b), (c) and (d).

After finding the pare pixels in the surrounding environment, their values have been followed during the mine operation to obtain confidence about the proposed method. In Figure 12 (a), (b) and (c), the variation of NDVI values of randomly chosen pixels with their pares is shown. These pixels (the chosen pixels) selected from the surrounding environment were not impacted by mining-influenced water. Hence, the NDVI values of them during mine activities should be almost similar to the NDVI values of their pares. By looking at them in more details, via looking at their line graphs in Figure 12 (a), (b) and (c), and doing Euclidian Distance or ED, this right was obtained. The ED for the pixel in Figure 9 (b) was almost 0.484, while other pixels in that area were more than this number. For instance, the ED values of this pixel with pixels, which were located in (height=61, width=305), (64,265), and (59,65), were 1.966, 2.152 and 2.368, respectively. Hence, 0.484 was the lowest amount, which means the closest variation domain during mine operation. In addition, the ED values for other couple pixels (Figure 12 (c) and (d)) were 0.491 and 0.497 in order.

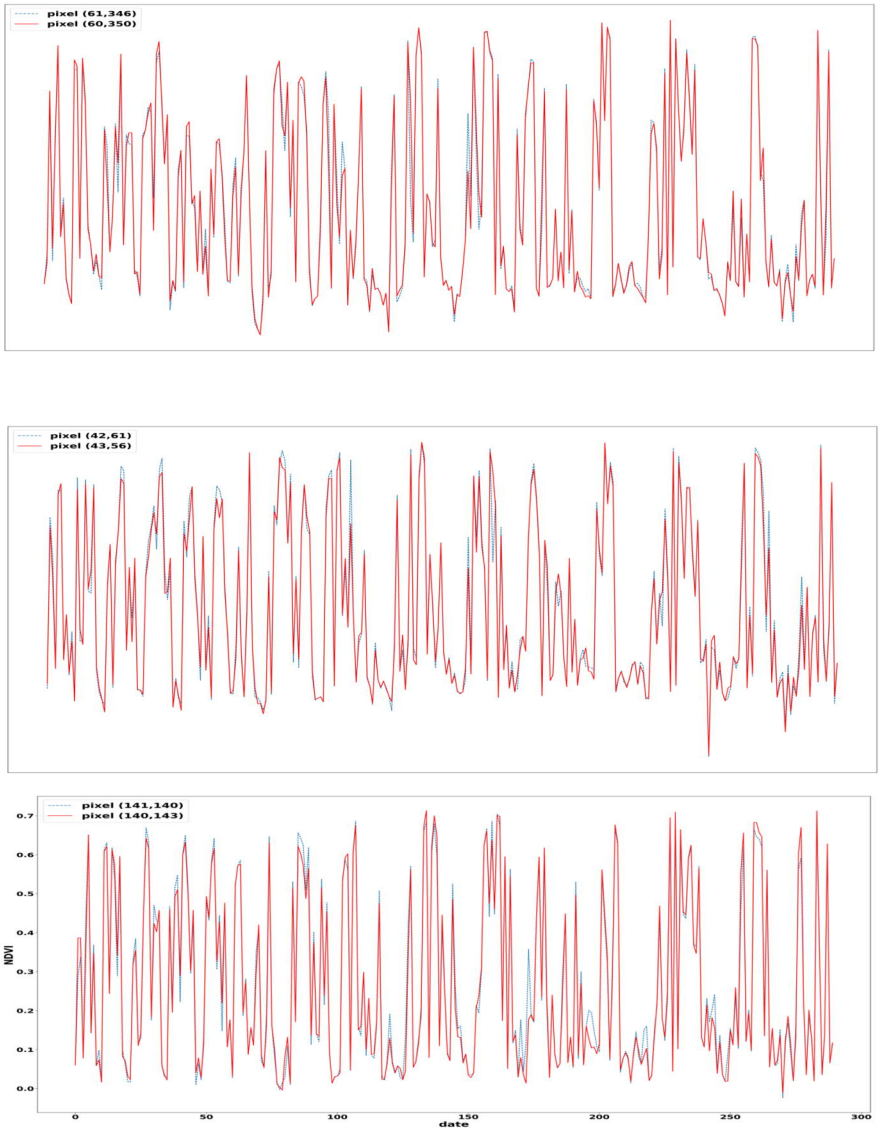

Figure 12. The NDVI values' changing line graph of chosen pixels with their pare pixels between 1993 and 2020 (NDVI values were computed through 290 images)

4.3. Estimating NDVI Values for All Pixels in TP-A and TP-B without Water Treatment Impacts

All in all, the goal of this study is estimating NDVI values for whole pixels in TP-A and TP-B and what values they would achieve without mining-influenced water affects during mining operation. As mentioned before the treatment operations of wastewater are different in both peatlands and each of them is doing separate treatment. Furthermore, the impacts of mining-influenced water through parts of TP-A and TP-B are different.

For predicting NDVI magnitudes or $NDVI_{el}$ for each pixel, which is located in TP-A or TP-B, mining extraction, the correlation coefficient, before water treatment activities, of it with all surrounding area's pixels will be computed and finally the highest coefficient would be extracted. In other words, with this model the corresponding pixels of pixels in TP-A and TP-B from surrounding area will be mined and during mining operation the NDVI magnitude changes of them are considered as $NDVI_{el}$ of pixels in the study wetlands.

As talked before, when the search step will be doing the two thresholds of 0.8 for Pearson coefficient and 0.05 for p-value are considered, and the pare pixels which have the values between this range are determined and finally through them the highest correlation coefficient and lowest p-value will be extracted. This operation has been done for both study peatlands and the coordinates of some couple pixels, which have highest correlation with each other, as following example. For instance, the pixel with coordinate of (1,71) in TP-A had the around 0.98 for Pearson coefficient and 8.98e-75 for and p-value with pixel, which is located in (40,150) in surrounding area, before mining operation.

4.4. The Water Treatment Impact Results on TP-A and TP-B

NDVI values, which is used to measure the vegetation cover in an area, even could be impacted by environmental factors such as rainfall, temperature, net radiation, transpiration, and anthropogenic activities; as mentioned before, the two essential factors are necessary for the photosynthesis of planets which are sunlight and temperature, which could not be removed from in analyzing of greenness measurements.

Furthermore, using NDVI gives this ability to analyze the greenness or vegetation cover in a target area in previous days, months, weeks, and even year, which depends on the area's situation; for instance, the area could be forest, desert, grassland, etc. As shown in Figure 9 and 10, the NDVI values have changed based on months before the mining operation, but it is not clear that how much effect that water treatment operation has through the study peatlands.

Since, according to the proposed method to solve the complexity of the impacts of mining-influenced water on NDVI values, the corresponding pixels of each pixel in target wetlands have been found. Therefore, at this time, the environmental conditions which would affect both NDVI magnitudes (the pixel in target areas and its corresponding) are the same. Moreover, as before, there is a high relationship between the pixels in TP-A and TP-B, and the same environmental conditions impact those pixels. So, for coming up to analyze the impact of water treatment operation, Equation 6 will be employed, where the value of $NDVI_{el}$ is the NDVI magnitude of the corresponding pixel in the surrounding area, while $NDVI_{il}$ is the NDVI value of a pixel, which has been impacted via mining-influenced water. All in all, as the $NDVI_{el}$ and $NDVI_{il}$ values have been obtained in the same conditions, so the environmental factors in Equation 6 will be removed.

Now, this technique helped the authors to come up with unpredictable environmental conditions and uncertain results. The Equation 3 have been employed on each pixel placed in impacted areas. The output of this equation is visualized in Figures 13 and 14 with different colours, and with analyzing these figures, the impacts of water treatment operation on peatlands could be followed up.

Generally, the final chapter is assigned to analyze the impacts of mining-influenced water on the target peatlands and talk about the pros and cons of the introduced methods. Furthermore how to combined with other techniques in future.

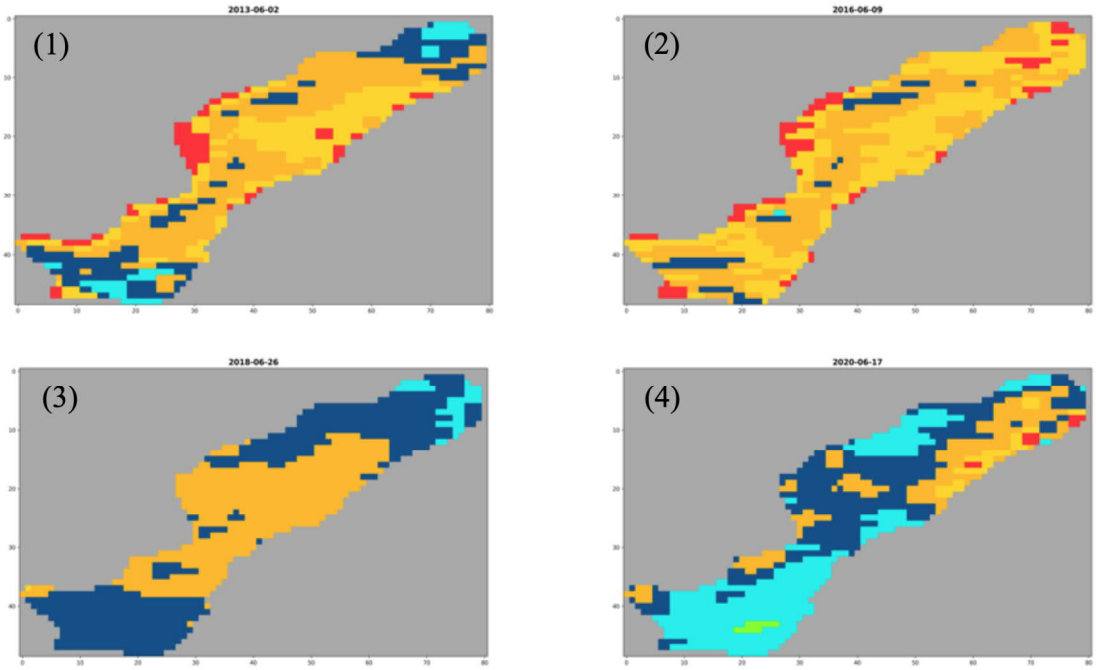
2013-06-02
(1)
2016-06-09
(2)
2018-06-26
(3)
2020-06-17
(4)

(a)

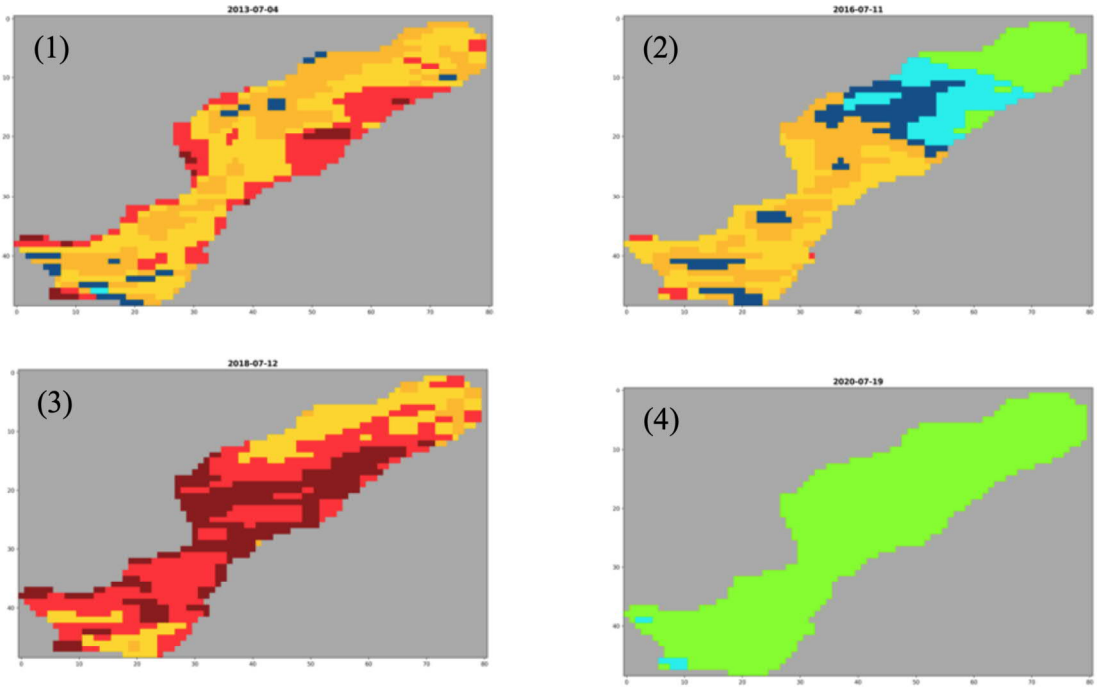
2013-07-04
(1)
2016-07-11
(2)
2018-07-12
(3)
2020-07-19
(4)

(b)

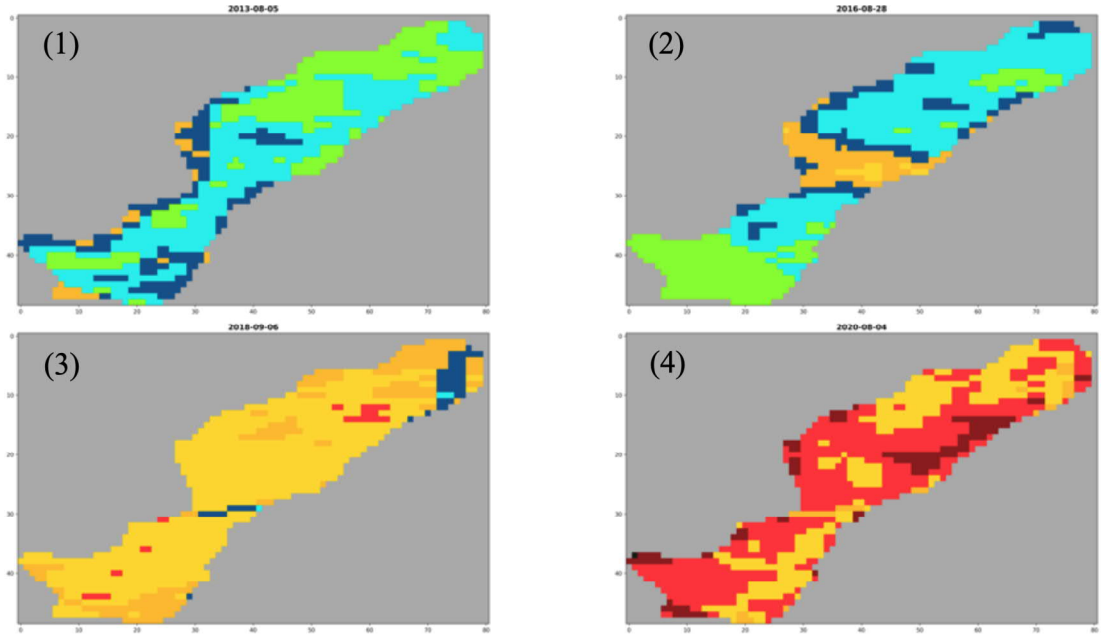

(c)

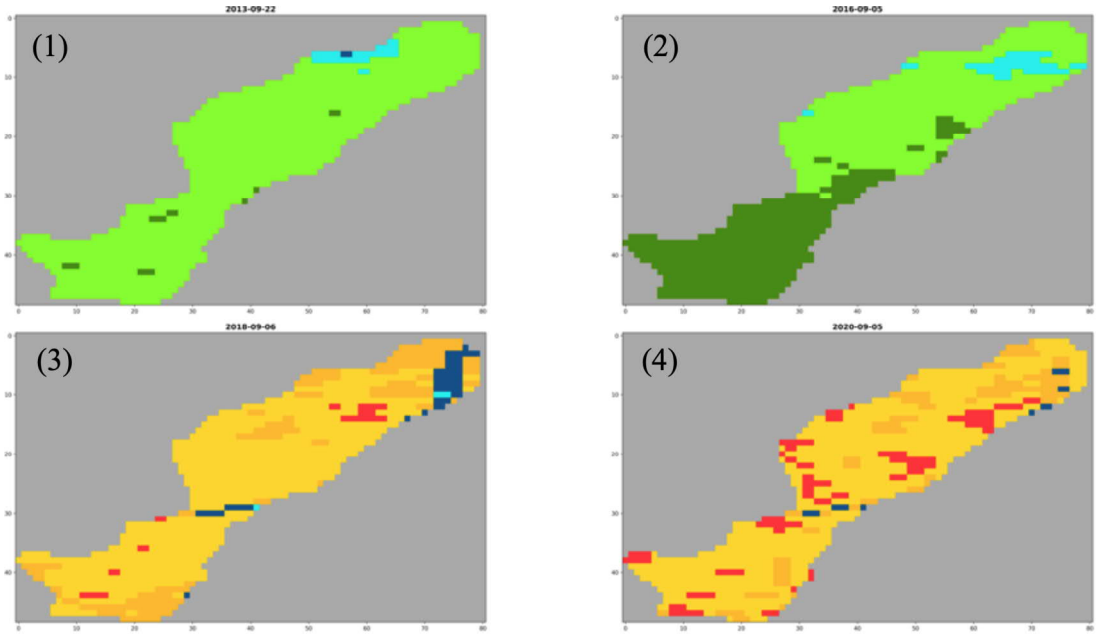

(d)

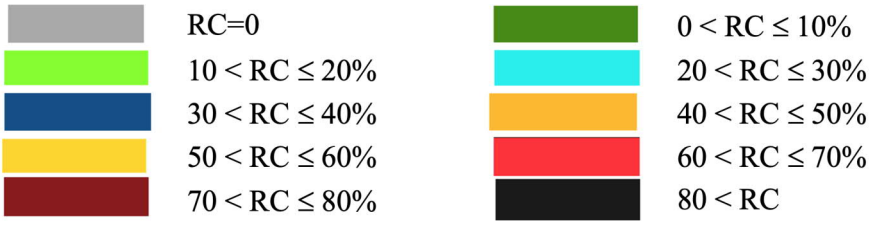

Figure 13. Relative change (RC) percentage between both NDVI values of each pixel in TP-A in four different years which are 2013, 2016, 2018 and 2020. (a) June; (1) 02/06/2013, (2) 09/06/2016, (3) 26/06/2018 and (4) 17/06/2020. (b) July; (1) 04/07/2013, (2) 11/07/2016, (3) 12/07/2018 and (4) 19/07/2020. (c) August; (1) 05/08/2013, (2) 28/08/2016, (3) 06/08/2018 and (4) 04/08/2020. (d) September; (1) 22/09/2013, (2) 05/09/2016, (3) 06/09/2018 and (4) 05/09/2020.

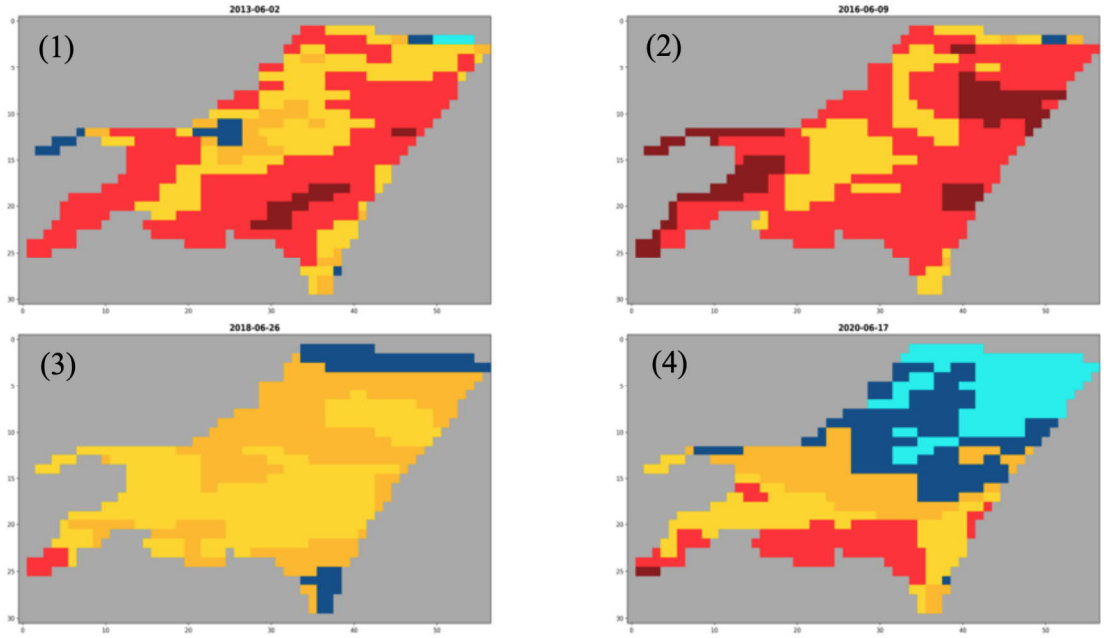
2013-06-02
(1)
2016-06-09
(2)
2018-06-26
(3)
2020-06-17
(4)

(a)

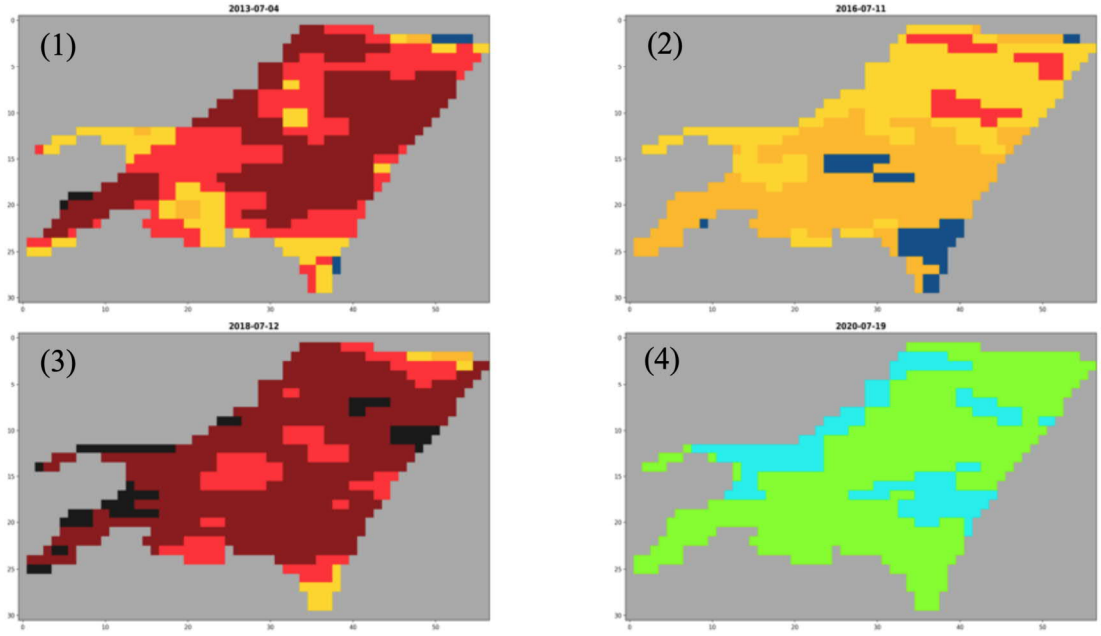
2013-07-04
(1)
2016-07-11
(2)
2018-07-12
(3)
2020-07-19
(4)

(b)

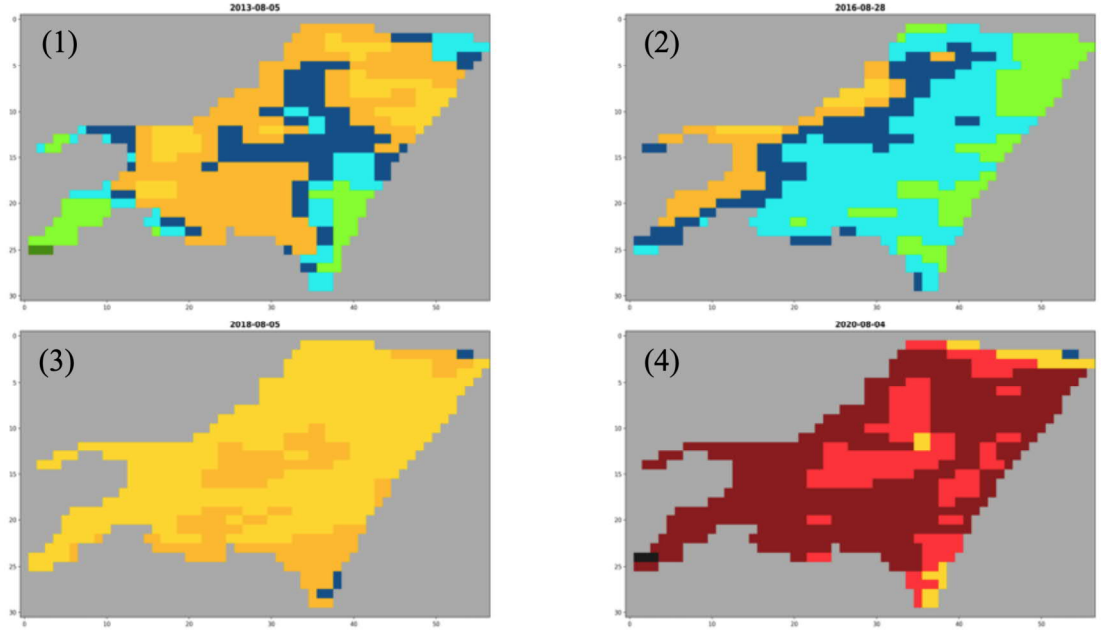

(c)

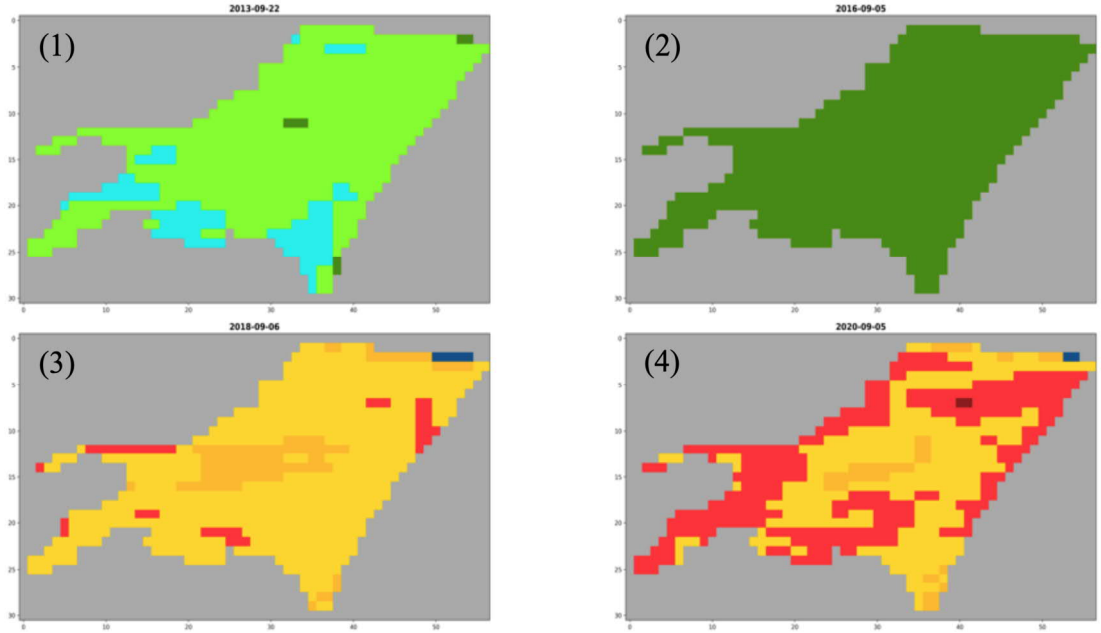

(d)

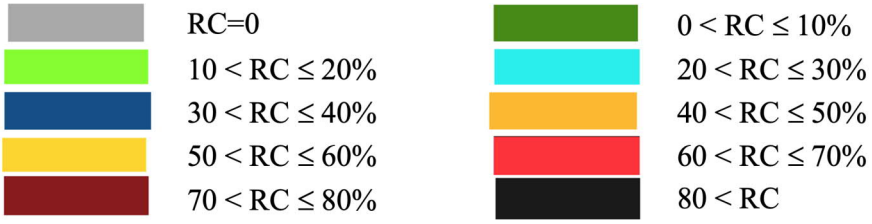

Figure 14. Relative change (RC) percentage between both NDVI values of each pixel in TP-B in four different years which are 2013, 2016, 2018 and 2020. (a) June; (1) 02/06/2013, (2) 09/06/2016, (3) 26/06/2018 and (4) 17/06/2020. (b) July; (1) 04/07/2013, (2) 11/07/2016, (3) 12/07/2018 and (4) 19/07/2020. (c) August; (1) 05/08/2013, (2) 28/08/2016, (3) 06/08/2018 and (4) 04/08/2020. (d) September; (1) 22/09/2013, (2) 05/09/2016, (3) 06/09/2018 and (4) 05/09/2020.

5. DISCUSSION

5.1. The Impacts of Mining-Influenced Water on TP-A and TP-B

As shown before (Figures 9 and 10), the months of June, July, August and September experienced a high level of NDVI in total compare to other months. Hence, these months (June, July, August and September) have been chosen as the target months for analyzing the results in this study.

First of all, the measurements of mining-influenced water impacts on TP-A and TP-B in June (Figures 13(a) and 14(a)). In 2013 (section 1), generally, the TP-A has better green cover than TP-B, and TP-B has been influenced more than TP-A, so this treatment operation was harmful to the peatland. In both target areas, the middle parts were impacted significantly with the impacts of mining-influenced water, while the edge parts have a better situation, especially the north and south of TP-A. Furthermore, in 2016 (Figures 13(a) and 14(a) section 2), the vegetation cover had been worse than in 2013 in both areas, but vs 2013 the middle parts in TP-A and TP-B was not more suffered via operation of water treatment, and the most impacted parts are located in the edges also, as 2013 TP-B was influenced more than TP-A in 2016.

Moreover, in June of 2018 (Figures 13(a) and 14(a) section 3), the vegetation cover in both target peatlands was better in comparison with previous years. In addition, again, the middle parts of both areas were more suffered from the impacts of the water treatment operation. Generally, the TP-B, like 2013 and 2016 were impacted more than TP-A, while it was not significant. However, in June of 2020 (Figures 13(a) and 14(a) section 4), something strange happened, and in that section, improvement of vegetation cover could be seen compared to the previous years. This improvement is significantly shown in TP-A, and even TP-B has experienced a vegetation cover improvement, but the south part still suffered from water treatment operation. Generally, same as previous comparisons, still TP-B had worse greenness cover compare to TP-A.

Over and over, the relative change percentages of each pixel in target wetlands in June of 2013 (Figures 13(b) and 14(b) section 1) shows a visible change of NDVI of each pixel in both areas. At this moment, both peatlands were suffered from the properties of mining-influenced water; especially this variation was so bad in TP-B. Additionally, this month was worse than June in the same year. Even though in 2016 (Figures 13(b) and 14(b) section 2), bit improvements are seen in both study environment compare to June in the same year, and the TP-B had a significant difference between NDVIel and NDVIil compare to TP-A. This improvement compares to the previous month might be due to the increase in rainfall, temperature or sunlight.

Frequently, the interesting point is about July of 2018 (Figures 13(b) and 14(b) section 3), which shows a significant change between real NDVI and whatever has been predicted. At this time, both study environments experienced great annoyance from mining-influenced water. When it compares to June of the same year, this

variation is so huge, and this impact was so earnest in PT-B, where some parts experienced a relative change percentage of more than 80%. Though, the NDVI values in both study zones have not been impacted with properties of wastewater of mining operation in July of 2020 (Figures 13(b) and 14(b) section 4). On this date, the relative change percentage presents a low variation in both study areas, while the rate of change in this again is more in TP-B than TP-A.

The third month, which is going to be interpreted, is August (Figures 13(c) and 14(c)). The first year is 2013 (Figures 13(c) and 14(c) section 1), which shows a not-markable relative change percentage in both target peatlands. On this date, the middle pixels of TP-B were suffered from water treatment operation compares to the other pixels, while in TP-A, just some pixel in the edges experienced a higher relative change percentage. Three years later (Figures 13(c) and 14(c) section 2), a notable improvement could be seen in TP-B, and most of the pixels, which experienced suffered from properties of mining-influenced water in 2013, had a better situation in relative change percentage, and just some pixels in edges had the similar situation as 2013. Whereas TP-A was not like TP-B and in comparison, with the same month in 2013, the pixels experienced an annoying problem with water treatment operation, and this change is considered in the middle pixels, which most of them had relative change percentage between 40% and 50%.

Frequently, in August of 2018 (Figures 13(c) and 14(c) section 3), the study wetlands were impacted with passive water treatment activities significantly. Approximately total pixels (except 5 or 6 pixels) in TP-B in this period experienced relative change percentages between 40% and 60%, which happened in TP-A also. However, in August of 2018, just a few pixels, which are located in the northeast of TP-A, were not impacted by the sewage of the gold mine. Additionally, in the same month in 2020 (Figures 13(c) and 14(c) section 4), the conditions of pixels in the target zones were so worse. The significant damage of NDVI values could be seen in TP-B, in which the most pixels of remote sensing image experienced the change from 60% to 80%, even some pixels had more than 80 percentage of NDVI change. The vegetation cover in TP-A was damaged via wastewater treatment, where the most NDVI value of pixels changed until 70%, in August of 2020.

The last month in which the high level of vegetation could be seen in September (Figures 13(d) and 14(d)). The first year was 2013 (Figures 13(d) and 14(d) section 1) when the study areas were not suffered via mining-influenced water as same as June, July and August in 2013. In addition, most pixels in TP-A and TP-B experienced a change between 10% and 20%, and around a a few pixels had changed under 30%. However, three years later (Figures 13(d) and 14(d) section 2), in August, the NDVI conditions had been better comparing to the same month in 2013, and the south part of TP-A and the whole area of TP-B the change is under 10%. In fact, this may happen due to the cloud, which the data was not valuable when captured.

All in all, in August of 2018 (Figures 13(d) and 14(d) section 3), both target wetlands experienced a notable change, and again the condition of TP-B is worse than TP-A. Also, two years later, which is 2020 (Figures 13(d) and 14(d) section 4), the

same problem happened in both areas, and most of their pixels experienced vegetation index change more than 40

In the end, what is noticeable about the water treatment process through TP-A and TP-B is that both target wetlands were damaged significantly in 2018 and 2020 (Figures 13 and 14). However, during June and July of 2020, the situation of both areas was good, and this might happen due to the noise problems, which makes the researchers unable to capture the correct data. Also, during the whole analysis process, the TP-B suffered more from the water treatment process than TP-A, which receives different water properties and water characteristics (it treats with mine process water flows).

5.2. Advantages and Disadvantages

As demonstrated by our study, vegetation cover analysis through remote sensing is an excellent approach to unfold environmental issues associated with mining operations. Yet, a significant challenge still exists that may halter the performance enhancement of such methods. This concerns the appropriate preparation of data. Capturing helpful data is a big issue facing remote sensing data because some conditions such as noise and cloud cover the target area and do not allow the satellite to capture the reflectance from the Earth surface. In this study, this problem existed, and it has not been ignored. For instance, the cloud covers were available in the images, which belonged to June of 2020, and the authors were not able to analyze the vegetation cover in these images. Additionally, this problem influenced the finding process of a couple of pixels.

Furthermore, another issue was associated with pixels that have the highest correlation with pixels in their neighbourhood. Hence, in this study, the central part of the corresponding pixels, which have the highest correlation with pixels in TP-A and TP-B, in surrounding areas were located around the boundary with target peatlands. Since these pixels, which are close to the study wetlands, might be affected by human activities or water treatment operation, extracting information from these pixels might not be reliable due to those might be influenced with human activities of wastewater of gold mine. Also, finding corresponding pixels in the surrounding area before the operation of the gold mine would be located in mine construction during mining extraction, so during the analysis, the NDVI values will be around 0.

All in all, besides mentioned above issues, we tried to represent a novel data mining model in the interpretation of satellite images to analyze the impact of mining-influenced water's treatment on vegetation cover since this model gave this ability to authors to follow the changes of NDVI magnitude during months when the chance of vegetation cover is more and clarified the amount of water treatment impacts on a wetland.

5.3. Future Work

Finally, the main goal of this study, which was proving the impacts mining-influenced water on a wetland or peatland and lead this area to be bare, has been achieved. The results of this study also illustrated that the gold extraction had changed the target peatlands. Hence, this approach would be developed on other analysis of human activity impacts on nature, such as peat extraction on peatlands, constructions on forests, etc.

However, the efficiency of methods to analyze the impacts of human activities or environmental conditions on nature, such as what has been introduced in this study, entirely depends on the resolution and existence of the taken images. For solving this problem, in future, this method can be combined with machine learning techniques to reconstruct noisy or missing data, which will lead to obtaining better results and views.

6. CONCLUSIONS

The metal extraction industry in Finland started in the 1950s, with more than a thousand of mine operations. Actually, besides the economic benefits of metal mining in Finland, the treatment operation of mining-influenced water is a big problem, and mostly it has been done as a passive treatment. Typically, in a such water treatment activity, we use peatlands or wetlands as a buffer for filtering the constituents of the mining' wastewater. However, this passive wastewater treatment has the potential to impact the peatlands and wetlands. Using the capacity of remote sensing data to monitor the impacts of mining-influenced water on the greenness of the peatlands or wetlands during mining operation has the potential to overcome this environmental impact, but also presents some inherent challenges due to the lack of relevant -background data- that will be used for comparison with impacted data.

A potential solution consists in using the data of other peatlands, which are not impacted via human activities associated to mining operations, peat extraction, etc. However, such comparison is also challenged by the timely variation of the environmental factors of these peatlands such as temperature, sunlight, and rainfall in different environments. In this study , we introduced a new data mining approach for correlating pixels of area influenced by wastewater by pixels from non-influenced area, and use the highest correlating pixels to map the environmental factors.

The study built on the availability of large scale image dataset from Landsat 7, 8 of the mining site and its surrounding over a large time window, which can provide insights to study the influence of the mining's wastewater in the vicinity area. For this purpose, the Normalized Difference Vegetation Index (NDVI), calculated directly from captured images of Landsat 7 and 8, compared between normal and impacted data during the mining operation, was employed. The results showed a remarkable change in study peatlands, which are used as buffers for passive treatment. In some time periods, it has been shown that few parts in the target areas were utterly modified by the impacts of mining-influenced water. In short, the study revealed that the continuation of this influence would transform the study of peatlands to bare environments in the future.

Also, this method can be deployed in other studies, concerned with the impacts of human activities on other green-lands such as forests, wetlands, among others. Besides, the study highlighted the importance of the resolution of the chosen images in influencing the accuracy of using this approach.

7. REFERENCES

[1] Ruokonen E. & Temmes A. (2019) The approaches of strategic environmental management used by mining companies in finland. Journal of cleaner production 210, pp. 466–476.

[2] Puustinen K. (2003) Suomen kaivosteollisuus ja mineraalisten raaka-aineiden tuotanto vuosina 1530–2001, historiallinen katsaus erityisesti tuotantolukujen valossa. Geological Survey of Finland, unpublished report M 10, pp. 3–578.

[3] Kauppila P., Räsänen M.L. & Myllyoja S. (2013) Best environmental practices in metal ore mining (metallimalmikaivostoiminnan parhaat ympäristökäytännöt) , pp. 1796–1637.

[4] Vasara H. (2018) State and outlook of the mining industry. sales , p. 35.

[5] Hernesniemi H., Berg-Andersson B., Rantala O. & Suni P. (2011) Kalliosta kullaksi–kummusta klusteriksi. suomen mineraaliklusterin vaikuttavuusselvitys. ETLA, Helsinki: Taloustieto Oy .

[6] Mononen T. & Sairinen R. (2021) Mining with social license: Case study of kylylahti mine in northern karelia, finland. The Extractive Industries and Society 8, p. 100744.

[7] Macdonald R.W., Barrie L.A., Bidleman T.F., Diamond M.L., Gregor D.J., Semkin R.G., Strachan W., Li Y.F., Wania F., Alaee M. et al. (2000) Contaminants in the canadian arctic: 5 years of progress in understanding sources, occurrence and pathways. Science of the Total Environment 254, pp. 93–234.

[8] Leppänen J.J., Luoto T.P. & Weckström J. (2019) Spatio-temporal impact of salinated mine water on lake jormasjärvi, finland. Environmental Pollution 247, pp. 1078–1088.

[9] Nordstrom D.K. & Alpers C. (1997) Geochemistry of Acid Mine Waters .

[10] Plumlee G.S., Smith K., Montour M., Ficklin W. & Mosier E. (1999) Geologic controls on the composition of natural waters and mine waters draining diverse mineral-deposit types. The environmental geochemistry of mineral deposits, Reviews in Economic Geology 6, pp. 373–432.

[11] Johnson D.B. & Hallberg K.B. (2005) Acid mine drainage remediation options: a review. Science of the total environment 338, pp. 3–14.

[12] ZINCK[1] J. & AUB B. (2010) Overcoming active treatment challenges .

[13] Taylor J., Pape S. & Murphy N. (2005) A summary of passive and active treatment technologies for acid and metalliferous drainage (amd). In: Fifth Australian workshop on acid drainage, vol. 2931, vol. 2931.

[14] McCarty P.L. (2018), What is the best biological process for nitrogen removal: when and why?

[15] Silvan N., Vasander H., Karsisto M. & Laine J. (2003) Microbial immobilisation of added nitrogen and phosphorus in constructed wetland buffer. Applied Soil Ecology 24, pp. 143–149.

[16] Luukkonen T., Heponiemi A., Runtti H., Pesonen J., Yliniemi J. & Lassi U. (2019) Application of alkali-activated materials for water and wastewater treatment: a review. Reviews in Environmental Science and Bio/Technology 18, pp. 271–297.

[17] Zhang L.y., Zhang L., Liu Y.d., Shen Y.w., Liu H. & Xiong Y. (2010) Effect of limited artificial aeration on constructed wetland treatment of domestic wastewater. Desalination 250, pp. 915–920.

[18] Hengen T.J., Squillace M.K., O'Sullivan A.D. & Stone J.J. (2014) Life cycle assessment analysis of active and passive acid mine drainage treatment technologies. Resources, Conservation and Recycling 86, pp. 160–167.

[19] Younger P.L., Banwart S.A. & Hedin R.S. (2002) Mine water: hydrology, pollution, remediation, vol. 5. Springer Science & Business Media.

[20] Skousen J., Zipper C.E., Rose A., Ziemkiewicz P.F., Nairn R., McDonald L.M. & Kleinmann R.L. (2017) Review of passive systems for acid mine drainage treatment. Mine Water and the Environment 36, pp. 133–153.

[21] Ronkanen A.K. & Kløve B. (2007) Use of stabile isotopes and tracers to detect preferential flow patterns in a peatland treating municipal wastewater. Journal of Hydrology 347, pp. 418–429.

[22] Hedin R.S., Watzlaf G.R. & Nairn R.W. (1994) Passive treatment of acid mine drainage with limestone. Tech. Rep. 6.

[23] Watzlaf G.R., Schroeder K.T., Kleinmann R.L., Kairies C.L. & Nairn R.W. (2004) The passive treatment of coal mine drainage. United States Department of Energy National Energy Technology Laboratory Internal Publication , pp. 1–72.

[24] Groudev S., Nicolova M., Spasova I. & Schutte R. (2003) Treatment of waters from a copper mine by means of a permeable reactive barrier. Fifty years of the University of Mining and Geology "St. Ivan Rilski 46, pp. 229–231.

[25] Vymazal J., Greenway M., Tonderski K., Brix H. & Mander Ü. (2006) Constructed wetlands for wastewater treatment. In: Wetlands and natural resource management, Springer, pp. 69–96.

[26] Ihme R. (1997) Pintavalutus turvetuotantoalueiden valumavesien puhdistuksessa. .

[27] Heikkinen K., Ihme R., Osma A.M. & Hartikainen H. (1995) Phosphate removal by peat from peat mining drainage water during overland flow wetland treatment. Tech. rep., Wiley Online Library.

[28] Allen S., Murray M., Brown P. & Flynn O. (1994) Peat as an adsorbent for dyestuffs and metals in wastewater. Resources, Conservation and recycling 11, pp. 25–39.

[29] Bunzl K., Schmidt W. & Sansoni B. (1976) Kinetics of ion exchange in soil organic matter. iv. adsorption and desorption of pb2+, cu2+, cd2+, zn2+ and ca2+ by peat. Journal of Soil Science 27, pp. 32–41.

[30] Gosset T., Trancart J.L. & Thévenot D.R. (1986) Batch metal removal by peat. kinetics and thermodynamics. Water Research 20, pp. 21–26.

[31] Räisänen M., Lestinen P. & Kuivasaari T. (2001) The retention of metals and sulphur in a natural wetland–preliminary results from the old otravaara pyrite mine, eastern finland. In: Proc Intern Conf Mining and the Environ, Skellefteå, Sweden, pp. 662–670.

[32] Sjöblom Å. (2003) Wetlands as a means to reduce the environmental impact of mine drainage waters. Ph.D. thesis, Linköping University Electronic Press.

[33] Brown P., Gill S. & Allen S. (2000) Metal removal from wastewater using peat. Water research 34, pp. 3907–3916.

[34] Pakarinen P. & Ruuhijärvi R. (1978) Ordination of northern finnish peatland vegetation with factor analysis and reciprocal averaging. In: Annales Botanici Fennici, JSTOR, pp. 147–157.

[35] Rydin H., Jeglum J.K. & Bennett K.D. (2013) The biology of peatlands, 2e. Oxford university press.

[36] Desrochers A. & van Duinen G.J. (2006) Peatland fauna. In: Boreal Peatland Ecosystems, Springer, pp. 67–100.

[37] Wyche N., Eilu P., Koppström K., Kortelainen V., Niiranen T. & Välimaa J. (2015) The suurikuusikko gold deposit (kittilä mine), northern finland. In: Mineral deposits of Finland, Elsevier, pp. 411–433.

[38] Aunola K., Aho A., Vidqvist M. & Pieskä V. Reverse osmosis technology to reduce fresh water consumption–case study. In: Agnico Eagle Finland.

[39] Khan U.A. (2020) Challenges in using natural peatlands for treatment of mining-influenced water in a cold climate: considerations for arsenic, antimony, nickel, nitrogen, and sulfate removal. Faculty of Technology .

[40] Yaraghi N., Ronkanen A.K., Haghighi A.T., Aminikhah M., Kujala K. & Kløve B. (2020) Impacts of gold mine effluent on water quality in a pristine sub-arctic river. Journal of Hydrology 589, p. 125170.

[41] Khan U.A., Kujala K., Nieminen S.P., Räisänen M.L. & Ronkanen A.K. (2019) Arsenic, antimony, and nickel leaching from northern peatlands treating mining influenced water in cold climate. Science of the Total Environment 657, pp. 1161–1172.

[42] Khan U.A., Kujala K., Planer-Friedrich B., Räisänen M.L. & Ronkanen A.K. (2020) Long-term data reveals the importance of hydraulic load and inflow water quality for sb removal in boreal treatment peatlands. Ecological Engineering 148, p. 105785.

[43] Larkins C., Turunen K., Mänttäri I., Lahaye Y., Hendriksson N., Forsman P. & Backnäs S. (2018) Characterization of selected conservative and non-conservative isotopes in mine effluent and impacted surface waters: implications for tracer applications at the mine-site scale. Applied Geochemistry 91, pp. 1–13.

[44] Palmer K., Ronkanen A.K. & Kløve B. (2015) Efficient removal of arsenic, antimony and nickel from mine wastewaters in northern treatment peatlands and potential risks in their long-term use. Ecological Engineering 75, pp. 350–364.

[45] Gao L., Wang X., Johnson B.A., Tian Q., Wang Y., Verrelst J., Mu X. & Gu X. (2020) Remote sensing algorithms for estimation of fractional vegetation cover using pure vegetation index values: A review. ISPRS Journal of Photogrammetry and Remote Sensing 159, pp. 364–377.

[46] Ge J., Meng B., Liang T., Feng Q., Gao J., Yang S., Huang X. & Xie H. (2018) Modeling alpine grassland cover based on modis data and support vector machine regression in the headwater region of the huanghe river, china. Remote Sensing of Environment 218, pp. 162–173.

[47] Jing X., Yao W.Q., Wang J.H. & Song X.Y. (2011) A study on the relationship between dynamic change of vegetation coverage and precipitation in beijing's mountainous areas during the last 20 years. Mathematical and Computer Modelling 54, pp. 1079–1085.

[48] Zeng X., Rao P., DeFries R.S. & Hansen M.C. (2003) Interannual variability and decadal trend of global fractional vegetation cover from 1982 to 2000. Journal of Applied Meteorology 42, pp. 1525–1530.

[49] Aggarwal S. (2004) Principles of remote sensing. Satellite remote sensing and GIS applications in agricultural meteorology 23, pp. 23–28.

[50] What is remote sensing? `https://earthdata.nasa.gov/learn/backgrounders/remote-sensing`. Accessed: 2021-05-22.

[51] Jordan C.F. (1969) Derivation of leaf-area index from quality of light on the forest floor. Ecology 50, pp. 663–666.

[52] Brown L., Chen J.M., Leblanc S.G. & Cihlar J. (2000) A shortwave infrared modification to the simple ratio for lai retrieval in boreal forests: An image and model analysis. Remote sensing of environment 71, pp. 16–25.

[53] Chen J.M. (1996) Evaluation of vegetation indices and a modified simple ratio for boreal applications. Canadian Journal of Remote Sensing 22, pp. 229–242.

[54] Tucker C.J. (1980) A spectral method for determining the percentage of green herbage material in clipped samples. Remote Sensing of Environment 9, pp. 175–181.

[55] Rouse J., Haas R.H., Schell J.A., Deering D.W. et al. (1974) Monitoring vegetation systems in the great plains with erts. NASA special publication 351, p. 309.

[56] Nemani R., Pierce L., Running S. & Band L. (1993) Forest ecosystem processes at the watershed scale: sensitivity to remotely-sensed leaf area index estimates. International journal of remote sensing 14, pp. 2519–2534.

[57] Gitelson A.A., Kaufman Y.J. & Merzlyak M.N. (1996) Use of a green channel in remote sensing of global vegetation from eos-modis. Remote sensing of Environment 58, pp. 289–298.

[58] Roujean J.L. & Breon F.M. (1995) Estimating par absorbed by vegetation from bidirectional reflectance measurements. Remote sensing of Environment 51, pp. 375–384.

[59] Crippen R.E. (1990) Calculating the vegetation index faster. Remote sensing of Environment 34, pp. 71–73.

[60] Vescovo L. & Gianelle D. (2008) Using the mir bands in vegetation indices for the estimation of grassland biophysical parameters from satellite remote sensing in the alps region of trentino (italy). Advances in Space Research 41, pp. 1764–1772.

[61] Huang S., Tang L., Hupy J.P., Wang Y. & Shao G. (2020) A commentary review on the use of normalized difference vegetation index (ndvi) in the era of popular remote sensing. Journal of Forestry Research , pp. 1–6.

[62] Khanh P.T., Ngoc T.T.H. & Thuong D.H. (2020) Application of landsat 8 image to extract waterline and build the relationship between chlorophyll-a and ndvi index for bung binh thien lake, southern vietnam , pp. 20–28.

[63] Cárdenas D.A.G., Valencia J.A.R., Velásquez D.F.A. & Gonzalez J.R.P. (2018) Dynamics of the indices ndvi and gndvi in a rice growing in its reproduction phase from multi-spectral aerial images taken by drones. In: International Conference of ICT for Adapting Agriculture to Climate Change, Springer, pp. 106–119.

[64] Kumar D. & Shekhar S. (2015) Statistical analysis of land surface temperature–vegetation indexes relationship through thermal remote sensing. Ecotoxicology and environmental safety 121, pp. 39–44.

[65] Normalized difference vegetation index. `https://en.wikipedia.org/wiki/Normalized_difference_vegetation_index`. Accessed: 2021-05-23.

[66] Gan T.Y. & Burges S.J. (2006) Assessment of soil-based and calibrated parameters of the sacramento model and parameter transferability. Journal of Hydrology 320, pp. 117–131.

[67] Zeng X., Dickinson R.E., Walker A., Shaikh M., DeFries R.S. & Qi J. (2000) Derivation and evaluation of global 1-km fractional vegetation cover data for land modeling. Journal of Applied Meteorology 39, pp. 826–839.

[68] Yang H. & Yang Z. (2006) A modified land surface temperature split window retrieval algorithm and its applications over china. Global and Planetary Change 52, pp. 207–215.

[69] Tan K.P., Kanniah K.D., Busu I.B. & Cracknell A.P. (2011) Evaluation of modis gross primary productivity of tropical oil palm in southern peninsular malaysia. In: 2011 IEEE International Geoscience and Remote Sensing Symposium, IEEE, pp. 756–759.

[70] Gutman G. & Ignatov A. (1998) The derivation of the green vegetation fraction from noaa/avhrr data for use in numerical weather prediction models. International Journal of remote sensing 19, pp. 1533–1543.

[71] Zaitunah A., Ahmad A., Safitri R. et al. (2018) Normalized difference vegetation index (ndvi) analysis for land cover types using landsat 8 oli in besitang watershed, indonesia. In: IOP Conference Series: Earth and Environmental Science, vol. 126, IOP Publishing, vol. 126, p. 012112.

[72] Autio J. & Heikkinen O. (2002) The climate of northern finland. Fennia-International Journal of Geography 180, pp. 61–66.

[73] Koppen W. & GEIGER R. (1936) Das geographische system der klimate handbuch der klimatologie. Ed. W. Koppen and R. Geiger 1.

[74] Schober P., Boer C. & Schwarte L.A. (2018) Correlation coefficients: appropriate use and interpretation. Anesthesia & Analgesia 126, pp. 1763–1768.

[75] Piao S., Fang J., Zhou L., Guo Q., Henderson M., Ji W., Li Y. & Tao S. (2003) Interannual variations of monthly and seasonal normalized difference vegetation index (ndvi) in china from 1982 to 1999. Journal of Geophysical Research: Atmospheres 108.

[76] Mao D., Wang Z., Luo L. & Ren C. (2012) Integrating avhrr and modis data to monitor ndvi changes and their relationships with climatic parameters in northeast china. International Journal of Applied Earth Observation and Geoinformation 18, pp. 528–536.

8. APPENDICES

8.1. Kittilä Gold Mine

The owner of Kittilä gold mine is called Agnico-Eagle Mines Ltd and this mine is sited close to a city named Kittilä, and far as 35 km. In 1986 the first discovering of gold in this environment happened, and between 1987 and 1997 more investigations were done. While The permission of water and environment for mine operation received in 2002, the mine construction started in 2006. The mine operation has begun with a pit in 2008 and the first extraction of gold from this mine happened in fall of this year. From the open pit the ore, which is combined with waste rock, is extracted then the waste rock is being separated from ore in a phase called loading.

Since 2010 the ore has been mined from underground operation as well as open pit operation, and the type of underground mining is bench stoping. Each stope may have a height between 25 and 40 meters and the mean size of it would be 10,000 tons of ore. A hardening fill will be added to the out stopes from mining after loading in term of filling, which makes it mined effectively and safely.

Next step is crashing the transported ore via jaw crusher in the concentrating plant, and then the output, which is crashed ore, is transmitted into a silo. In the next step, the ore will be ground with using semiautogenous grinder and then the finely ground ore moves on the two floating stages. In the first stage from the slurry concentrate the organic carbon would be separated, and in the second stage the sulphide minerals, which include gold, are recovered. After this step, the oxidation of slurry is produced with an autoclave which has 190°C temperature and 1900 kPa pressure. Then the concentrate, which is oxidized, in the circuit of leaching gold is provided. With using six leaching tanks (CIL tank), the concentrate rests trough them in period of 24 hours and makes the extraction of gold. Also, active carbon is used in order to recover the dissolved gold. In the continues, the active carbon includes gold is separated and the gold will be extracted via electrowinning, then the gold would be warmed to be melt and then cold operation would be executed to produce doré bars. Furthermore, the extra operation is being done on bars outside company and the final production has quality of 99.99%.

water-tight tailings ponds include the tailings, which are produced through concentrating stage, and the number of of these tailings are equal to the amount of ore, which is transformed to the plant of concentrate. In addition, the waste rock is put in storage area, which is considered for waste rock.

8.2. Mann-Kendall Trend Test

Mann-Kendall trend test is a practical test to understand statistically remarkable raising or lowing down trend through a period of time. In Mann-Kendall, two hypothesis, one for testing that there is a trend or not and called null hypothesis(H0), and other declares the remarkable raising or lowing down trend in during a period of time, which is called alternative hypothesis (H1).

Mann-Kendall trend test is used to find the trend through any dataset of data points which contain more than 4 contents. Hence, when the number of points is less than four, Mann-Kendall trend test would be able to find the trend, even there is a trend. All in all, the main goal of using Mann-Kendall trend test is finding the possible differences in data.

8.3. Source-Code of Capturing Data

```
// Provide GEE user's feature location
var Kittila_Mining = ee.FeatureCollection("....");
var batch = require('users/fitoprincipe/geetools:batch');
// Using Landsat 8 for example
var landsatCollection = ee.ImageCollection("LANDSAT/LC08/C01/T1_8DAY_NDVI")
    .filterDate('2020-01-01', '2020-12-31')
    .filterBounds(Kittila_Mining)
    .map(function(image){return image.clip(Kittila_Mining)});

print (landsatCollection, "landsatCollection")

Map.centerObject(Kittila_Mining);
Map.addLayer(Kittila_Mining,{},'Kittila_Mining');

// provide your google drive location
batch.Download.ImageCollection.toDrive(landsatCollection,
                  '.....',
                  ({scale: 30,
                   fileFormat: 'GeoTIFF',
                   region: Kittila_Mining,
                   formatOptions: {
                    cloudOptimized: true}
                  }))

// Downloading all images automatically from GEE to the folder location of Google Drive
function runTaskList(){
    var tasklist = document.getElementsByClassName('task local type-EXPORT_IMAGE awaiting-user-config');
    for (var i = 0; i < tasklist.length; i++)
        tasklist[i].getElementsByClassName('run-button')[0].click();
}

function confirmAll() {
    var ok = document.getElementsByClassName('goog-buttonset-default goog-buttonset-action');
    for (var i = 0; i < ok.length; i++)
        ok[i].click();
}

runTaskList();
confirmAll();
```

8.4. Source-Code Finding Highest Correlation in TP-A

```
# Keeping non nan and non zero value index of north affected part
north_non_zero_indices=[]
# Keeping the index of high correlation in inverted images
north_inverted_match = []
# Keep high correlaion between two pair raws
north_inverted_max_corr = []
north_inverted_p= []
# Read each raw of north imapcted
for i in range(north_find_corr.shape[0]):
  #create empty array of to hold all correaltion
  max_corr =[]
  # To hold all j which are not zero or nan
  n=[]
  p=[]
  # read the raw of north impacted
  nn = np.array( north_find_corr.loc[i,:])
  # check where are the nan value
  where_are_NaNs = np.isnan(nn)
  # change nan value to zero
  nn[where_are_NaNs] = 0
  # check if the whole zero is zero
  is_all_zero = np.all((nn==0))
  # if it is not zero keep continue
  if  is_all_zero!=True:
    # append non-zero i
    north_non_zero_indices.append(i)
    print(i)
    #Read inverted matrix
    for j in range(inverted_find_cor.shape[0]):
      ii = np.array( inverted_find_cor.loc[j,:])
      where_are_NaNsii = np.isnan(ii)
```

8.5. Source-Code Finding Highest Correlation in TP-B

```
# Keeping non nan and non zero value index of north affected part
south_non_zero_indices=[]
# Keeping the index of high correlation in inverted images
south_inverted_match = []
# Keep high correlaion between two pair raws
south_inverted_max_corr = []
south_inverted_p= []

# Read each raw of north imapcted
for i in range(south_find_cor.shape[0]):
  #create empty array of to hold all correaltion
  max_corr =[]
  # To hold all j which are not zero or nan
  n=[]
  p=[]
  # read the raw of north impacted
  nn = np.array( south_find_cor.loc[i,:])
  # check where are the nan value
  where_are_NaNs = np.isnan(nn)
  # change nan value to zero
  nn[where_are_NaNs] = 0
  # check if the whole zero is zero
  is_all_zero = np.all((nn==0))
  # if it is not zero keep continue
  if  is_all_zero!=True:
    # append non-zero i
    south_non_zero_indices.append(i)
    print("Non Zero in South: ",i)
    #Read inverted matrix
    for j in range(inverted_find_cor.shape[0]):
      ii = np.array( inverted_find_cor.loc[j,:])
```